

UNIVERSITY OF HULL

**Analysis of the fume produced
during laser-material interactions**

by

A. E. Bridgwater, BSc.

being a thesis submitted for the
degree of Master of Science (by Research)

in the
Faculty of Science and Engineering
Department of Physics

April 2020

Abstract

The purpose of this research was to improve knowledge of the by-products of laser processing; namely the composition of particles, gases and vapours that are evolved during laser-material interactions. For IR sources, photothermal processes occur and thermal degradation products result, whereas UV lasers may additionally induce photochemical effects. The material investigated was an ITO ink (indium tin oxide nanoparticles in a photo-curable binder and organic solvent) spin-coated onto glass substrates. Thermogravimetric analysis showed that even for temperatures below the upper working limit of the glass substrate, gas-phase products are produced. Laser heating of the binder, 3-methacryloxypropyl-trimethoxysilane (MPTS), in a closed chamber showed that infrared irradiation generates butyl methacrylate. In order to collect a sample representative of the fume entrained in a local exhaust ventilation (LEV) system, an isokinetic arrangement was developed. This balances the volumetric flow rates of the main extraction flow and a sampling tube so that both experience the same flow velocity. Gases were collected with this system into a Tedlar bag and then adsorbed onto a solid phase microextraction (SPME) fibre followed by GC-MS analysis. However, contamination from polymers in the sampling system was detected and so a glass/metal construction was utilized in the final version. The gas phase data were inconclusive as no peaks above the detection limits of the equipment could be attributed to laser interactions. The cause of this has been tentatively attributed to excessive dilution of the analytes. Through SEM and EDXA measurements, particulates captured following $130\text{mJ}/\text{cm}^2$ XeCl laser irradiation were successfully identified

as 40nm ITO particle clusters. It is concluded that the use of a three-stage LEV system is advisable with pre-filter, HEPA filter, and activated charcoal. A flow rate of at least 150m³/hr is recommended, and personal monitoring is advised.

Acknowledgements

I would like to thank my supervisor, Dr Howard Snelling for his continued patience during this project. Also to Dr Kevin Welham for his willingness to share equipment and ideas, and for always answering my unlimited questions. Thank you also to my parents, the postgraduate office, Carl, and Michelle for their support and pep talks.

And finally, thank you to my fellow Indium Free Innovative Technology (INFINITY) colleagues Jack, Rob, Anton, and all of the project partners for welcoming me to the party.

This work was conducted as part of the INFINITY project which was funded from the European Unions Horizon 2020 Research and Innovation Programme under grant agreement No. 641927.

Contents

Abstract	ii
Acknowledgements	iv
Glossary of Abbreviations	vii
1 Introduction	1
2 Literature review	4
2.1 Introduction	4
2.2 UV laser irradiation	5
2.3 IR laser irradiation	6
2.4 Gas sampling techniques	10
2.4.1 The isokinetic condition	11
2.4.2 Sample concentration	12
2.4.3 Sample transfer and Tedlar bag sampling	14
2.5 Particulate capture techniques	16
2.6 Conclusion	18
3 Materials	20
3.1 Introduction	20
3.2 Nanoparticles	21
3.3 Binder	22
3.4 Solvent	25
3.5 Substrates	26
3.6 Ink	29
3.7 Coating techniques	31
3.7.1 Spin-coating	32
3.8 Conclusion	32
4 Static Sampling	34
4.1 Introduction	34
4.1.1 Background to the experimental techniques	34
4.2 Optimisation of the GC-MS method	39

4.3	Direct chamber sampling	44
4.4	Results	46
4.5	Discussion	49
4.6	Conclusions	51
5	Dynamic Sampling	52
5.1	Introduction	52
5.2	Chamber cross-flow sampling	53
5.2.1	XeCl laser irradiation	55
5.2.2	RF:CO ₂ laser irradiation	58
5.3	Direct cross-flow sampling	59
5.4	Gas capture	61
5.4.1	Tedlar bag sampling	63
5.4.2	Glass chamber sampling	68
5.4.2.1	XeCl laser irradiation	70
5.4.2.2	RF:CO ₂ laser irradiation	74
5.4.3	Discussion	76
5.5	Particulate sampling from a gas flow	78
5.6	Discussion	80
5.7	Conclusion	81
6	Hazard Assessment	83
6.1	Introduction	83
6.2	Review of MSDS data	83
6.2.1	ITO nanoparticles	84
6.2.2	Isopropoxyethanol	85
6.2.3	MPTS	85
6.2.4	Butyl methacrylate	86
6.2.5	N-dimethyl acetamide	87
6.2.6	Octamethylcyclotetrasiloxane	88
6.2.7	Phenol	89
6.3	Analysis of the hazards	90
6.4	Conclusion	92
7	Conclusion	93
	References	98

Glossary of Abbreviations

AC	Alternating current
Al ₂ O ₃	Aluminium oxide
ArF	Argon fluoride
B ₂ O ₃	Boron trioxide
C ₂	Diatomic carbon
CAS	Chemical Abstracts Service
CN	Cyanide
CO ₂	Carbon dioxide
CRM	Critical raw material
DC	Direct current
DVB/CAR/PDMS	Divinylbenzene/carboxen/polydimethylsiloxane
EDXA	Energy dispersive X-ray analysis
GC	Gas chromatograph/y
GC-MS	Gas chromatography-mass spectrometry
HCN	Hydrogen cyanide
HEPA	High-efficiency particulate air
HPLC	High-performance liquid chromatography
ID	Internal diameter
INFINITY	Indium Free Innovative Technology
INM	Leibniz Institute for New Materials
IPE	2-Isopropoxyethanol
IR	Infrared
ITO	Indium tin oxide
LC50	Median lethal concentration
LD0	Maximum tolerable concentration

LD50	Lethal dose 50%
LDLO	Lowest lethal dose
LEV	Local exhaust ventilation
MPTS	3-Methacryloxypropyltrimethoxysilane
MS	Mass spectrometer
MSHA	Mine Safety and Health Administration
Na ₂ O/K ₂ O	Sodium oxide/potassium oxide
NaCl	Sodium chloride
NIOSH	National Institute for Occupational Safety and Health
PET	Polyethylene terephthalate
PPE	Personal protective equipment
PTFE	Polytetrafluoroethylene
PVC	Polyvinyl chloride
RF:CO ₂	Radio frequency carbon dioxide
SEM	Scanning electron microscope
SIM	Selected ion monitoring
SiO ₂	Silicon dioxide
SPME	Solid phase microextraction
STEL	Short term exposure limit
TCOs	Transparent conductive oxides
TGA	Thermogravimetric analysis
TWA	Time weighted average
UV	Ultraviolet
VOCs	Volatile organic compounds
WP	Witness plate
XeCl	Xenon chloride

Introduction

The role of lasers in manufacturing industries is increasing and will continue to do so [1–3]. It is necessary, therefore, to improve knowledge of laser processing by-products so as to mitigate any hazards. Laser generated fume is the combination of substances released from a material during irradiation. Fume consists of permanent gas phase and condensing emissions, as well as particulate ejecta.

During laser processing, fume is produced at the interaction site by photothermal and photochemical ablation processes. In the photothermal case, energy absorbed from the laser irradiation manifests as heat, and causes evaporation via the production of volatile species. Alternatively, interaction with irradiation from lasers that produce photons higher in energy than molecular bonds can induce photo-induced bond scission, which breaks bonds in the material causing the release of volatile products. The chemical composition of fume therefore originates from the decomposition products of materials processed at the interaction site via these ablation processes. It is possible that volatile material produced as gas phase in the elevated temperatures near the interaction site, can undergo adiabatic expansion and form condensed droplets as the vapour cools.

It is necessary to develop techniques and processes to capture and analyse gases and particulates released from the laser interaction site so that potential hazards can be identified.

Areas of technological growth are electronic displays and photovoltaic devices that require flexible, transparent, and conductive electrodes. Commonly used materials in these devices include transparent conductive oxides (TCO's) such as indium tin oxide (ITO). ITO is most commonly used in thin film form, principally as transparent electrodes for solar cells and liquid crystal displays. ITO is the most commonly used form of indium, a scarce metallic element. Indium has been classed as a Critical Raw Material (CRM) leading to substantial price increases over recent years. It is predicted that the global supply of indium will be exhausted within the coming decade [4]. Therefore, it is necessary to reduce the use of indium now and develop indium-free technologies for the future. Methods of reducing ITO usage include avoiding wastage and streamlining manufacturing processes, such as ink-jet printing ITO solution-based inks followed by laser sintering. Success in developing such ink-laser heat treatment procedures will result in large-scale fume output from device manufacturers.

The objective of this thesis is two-fold. To develop particulate and gas phase fume sampling techniques, and to analyse the fume composition resulting from laser processed next-generation ITO inks. In this way, the subsidiary aim of determining if the fume is harmful will be enabled.

The structure of this thesis is as follows. Firstly, a literature review will discuss the emissions from various laser-material interactions. Current industrial scale laser filtration will also be considered and sampling techniques related to the laser processing of materials will be described. Literature describing the materials that will be laser irradiated will be explored, and the substances produced from previous

laser fume analyses reviewed. Finally relevant analysis techniques will be discussed and described for the laser fume analysis approach.

Chapter 3 introduces and characterises the materials involved in laser irradiation of wet processed ITO inks. This involves the components of the printed structures used in this project such as the ITO nanoparticles, 3-Methacryloxypropyltrimethoxysilane (MPTS) binder and isopropoxyethanol solvent.

Chapter 4 describes the premise and development of *static sampling*. Static sampling encompasses closed cell systems or those with no extraction. This means fume created via laser processing is not transported in an ambient gas flow and is therefore accumulated for analysis. Results are discussed for the solid-phase microextraction (SPME) fume analysis of the radio frequency carbon dioxide (RF:CO₂) (10.6 μ m) laser-material interactions.

Chapter 5 covers *dynamic sampling* which involves the sampling of fume from an extraction flow. The development of this method is shown to be analogous to extraction systems in the work place and the results are therefore relevant to sampling in the manufacturing industry. Results will be discussed for the RF:CO₂ laser (10.6 μ m), xenon chloride (308nm), and argon fluoride (193nm) lasers with regards to particulates and gaseous output from laser-material interactions.

In Chapter 6 a hazard assessment is performed for the substances identified from sampling techniques in chapters 4 and 5.

Finally, chapter 7 reviews outcomes of earlier chapters and draws further conclusions. Future work is suggested and discussed.

Literature review

2.1 Introduction

Knowledge of the composition of any fume in the manufacturing work place is important so as to ensure the safety of the employees. However, the aim of most literature that has measured gas and particulates has been to investigate the laser interaction mechanism, whereas little literature has been concerned with health and safety and hazard assessment in the workplace. In 1995, two thirds of factories did not measure the quantity of hazardous by-products produced by laser processing [5]. By monitoring emissions before and after processing, the effects of enclosure design, extraction and filtration can be ascertained. In order to ensure that the appropriate extraction and filtration is used, knowledge of the quantity and type of fume is needed. The forms in which laser-produced fume can occur include particulates, aerosols, gases, smoke and condensed vapour [5, 6]. It has been verified that when irradiating plastics, 90% of the particulates produced are less than $1\mu\text{m}$ in diameter [5]. The cause is not clear, however, regulations demand further pre-production testing. This poses serious risks to persons exposed to this fume as the nanoparticles can be aspirated into the lungs [5]. There is some work specifically on fume safety in the medical industry [7–9], and from the health and safety direction of the employees [5, 6, 10].

In this chapter the literature regarding the by-products produced during ultraviolet (UV) and infrared (IR) laser irradiation of materials will be reviewed. In order to identify these chemicals they will first have to be collected. Therefore several techniques to sample both gas-phase and particulates will be described.

2.2 UV laser irradiation

There are many instances of laser fume generation in many experiments such as laser etching of polymers. Laser ablation of polyimide was completed at both 193nm and 308nm to study the mechanism of this process and perform chemical analysis of the products via laser-induced fluorescence analysis. The only product condensable at room temperature was carbon, both diatomic carbon (C_2) and cyanide (CN) were observed along with hydrogen cyanide (HCN). Srinivasan et. al. deduced that one photon absorbed by one monomer was not sufficient to produce ejecta, and in fact it takes many photons absorbed per monomer to eject small products (less than 4 atoms) at supersonic velocities [11]. It follows using lasers of the same wavelength at a fluence of at least $0.08J/cm^2$ and pulse duration of 50ns [11] on polymer films, carbon-based ejecta might be observed. The ejecta were observed to leave the surface at a solid angle of 30° [11].

Creasy et. al. observed large carbon cluster ions ($m/e > 800amu$) which showed parallels in the mass spectrometry of soot generation in flames [12]. These were formed from the irradiation of polyimide and graphite with a laser wavelength of

266nm and pulse duration of 10ns. The fluence used was 0.5-1J/cm² and caused 4x10¹³ atoms of carbon to be ablated [12].

Gotz et. al. found that when irradiating solid indium at 248nm with 15ns pulses, the ablation threshold was 100mJ/cm². Neutral indium atoms were found to eject in a perpendicular direction to the irradiation [13].

2.3 IR laser irradiation

When collecting laser generated fume, it would not be effective to merely have the collection system in the same laboratory as the laser interaction site. Therefore a distance must exist from which an adequate sample can be collected. It has been shown that a fume evacuation system is only effective if situated within a short distance of the laser interaction site [7]. Smith et. al. [7] used a 30W continuous wave laser with a spot size 0.5-1.0mm at the surface, to simulate smoke produced during surgery. The extraction unit used had a nominal flow rate of 1.4 m³/min with high-efficiency particulate air (HEPA) filters rated for 99.97% capture of 0.3μm particles.

An ‘oblong shaped nozzle’ was used approximately 50mm from the laser interaction site. They also used aerosol monitors to estimate the fume concentrations at distances in the region of 1m from the laser interaction site. The assumed area of the nozzle during their ventilation calculations was approximately 9.5cm² for a round opening. They also indicate that further study is needed with nozzles of different designs [7]. It was found that 100% of fume was captured with the above

apparatus approximately 50mm from the laser site. The authors did not specify the particles size but evacuators able to collect particles efficiently down to $0.1\mu\text{m}$ are recommended.

In another study, Smith et. al. [8] found that ambient airflow greatly affected the efficiency of fume collection. If the external flow was in the same direction as the extraction nozzle flow, very efficient collection occurred, however ambient flow at any other angle greatly affected the capture of emissions as a function of distance from the laser site [8]. The laser used was a continuous wave CO_2 with spot size 0.5-1.0mm at the surface. The irradiance levels used were between 3.8-50kW/cm² [8]. The size of particulates captured was not noted by the authors. With an increase in laser power, an increase in air flow speed was also needed to overcome greater fume release velocity, and the nozzle needed to be closer to the laser interaction site [8]. The highest efficiency of fume collection was found to be when the nozzle was as close as possible to the laser interaction site [8] however other literature states that fume will be collected within a distance of 1.5D (fig. 2.1), where D is the internal diameter of the nozzle.

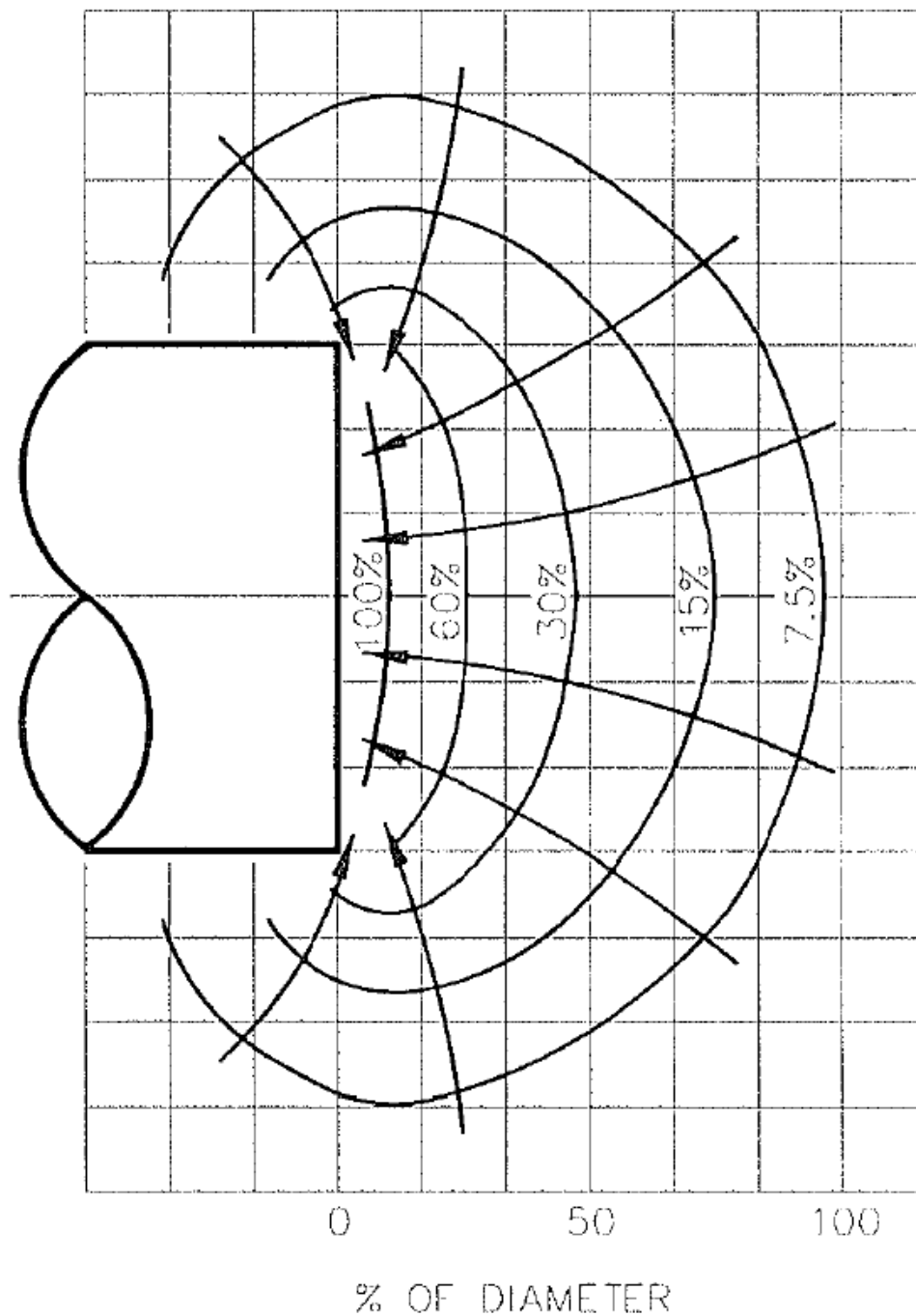


FIGURE 2.1: Velocity contours of a plain circular opening as a function of diameter percentage. It shows the velocity decreases inversely with the square of the distance from the opening [14].

Laser cutting of various plastics was completed and a qualitative report of the fume produced by Sims et. al. [15]. The production of hydrocarbon aromatic

rings was found along with evidence of particulate matter. A continuous 1500W carbon dioxide (CO₂) laser was used with a zinc selenide lens of focal length 125mm, and a beam diameter of 1mm. The speed was 4m/min and the laser power was set to 750W [15]. The particulate material was collected on glass fibre filters situated 300mm from the interaction site along with thermal and charcoal adsorption tubes. All the fume collection equipment was situated within a cabinet surrounding the laser interaction which consisted of a box with one outlet for the extraction flow, and a 10mm gap for fresh air to enter. The dimensions of the cabinet were 1.8x1.8x1.9m. The extraction equipment was not turned on until the fume had dispersed within the cabinet for 2 minutes. After 3 minutes the cabinet was opened for the next sheet of material to be cut [15]. For analysis, the filters were weighed before and after sampling to determine the weight gain. The Tenax adsorption tube was thermally desorbed and the sample flowed through a gas chromatography-mass spectrometry (GC-MS) instrument with quadropole mass spectrometer. The sample was solvent-desorbed from the charcoal tube with methanol and carbon disulphide and then introduced to the GC-MS. The oven temperature ramp was increased by 5°/min from 50°C to 250°C. The column used was non-polar bonded phase column [15]. When laser cutting polyethylene terephthalate (PET) in argon, 8.46mg of particulate material was collected from the glass filters [15].

Laser processing of 3mm thick polyvinyl chloride (PVC) was undertaken with a 300W continuous CO₂ laser at a feed rate of 4m/min. Air was used as an assist gas at 50psi through a nozzle diameter of 1mm [6]. A fume box was developed

that encapsulated the laser output, machining table and included a pipe to the extractor. The main fume components identified were hydrogen chloride, methyl methacrylate and benzene. Hydrogen chloride (HCl) is dangerous as it can cause burns to the skin and corrosion of equipment. It was found that 80% of the emissions were particulates $0.02\text{-}0.2\mu\text{m}^3$ in size [6]. The extraction flow was $0.5\text{m}^3/\text{s}$ with a velocity of $2.6\text{m}/\text{s}$. The extraction was through a honeycomb mesh 3.2mm in size with a depth of 40mm . The aim of this set up was to create a laminar flow within the fume box, however due to the large components within the box, only a turbulent flow was induced [6].

2.4 Gas sampling techniques

The by-products produced by the UV and IR irradiation of materials can include gases and/or vapour. The identification of these chemicals is difficult as there is much dilution of the sample in an extraction flow. Vassie et. al. determined that the fume must be contained to be analysed [6]. Laser irradiation inside a chamber is the easiest way to concentrate and collect fume. A material is placed in an air-tight chamber with an appropriate window (e.g. sodium chloride (NaCl) window for a wavelength of $10.6\mu\text{m}$) and the fume is accumulated during irradiation. However, this method is not analogous to large scale irradiation or processes involving high pressure assist gases [6]. Conversely, if a sample is collected from an extraction flow, it may be possible to quantify how much fume it contains by creating an isokinetic condition.

2.4.1 The isokinetic condition

In order for fume sampling to be representative of the main extractor flow, it is advantageous to consider the isokinetic condition [16]. In this way particulates are entrained and sampled in a controlled way allowing the potential for quantitative analysis. The general idea is that the sample flow rate in the probe tube (figure 2.2) is balanced to give the same flow velocity as the fume extractor pipe. In figure 2.2 the impact a difference in velocity between the sample pipe and the extraction pipe will have is illustrated, either collecting too much sample or forcing the flow around sample pipe opening. Whilst it is not a problem to sample too much fume, the sample will not be collected isokinetically in this instance.

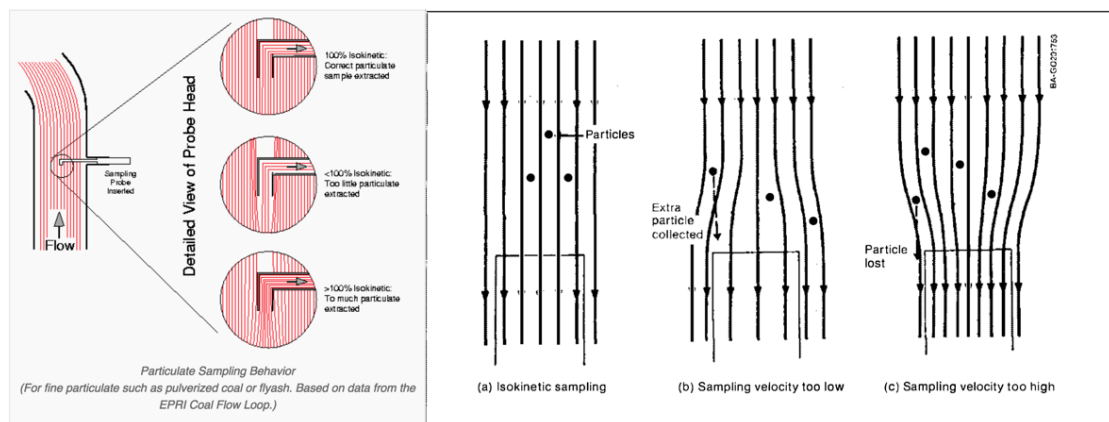


FIGURE 2.2: Two figures showing the isokinetic condition and alternatives. If the flow velocity in the sample pipe is too high, more fume and particulates are collected. However if the sample velocity is too slow, then not enough fume is collected and will not enter the sample pipe. [17] [16]

The flow velocity through a pipe is related to the volumetric flow rate via equation 2.1 [18].

$$V_x = \frac{Q_x}{\pi(D_x/2)^2} \quad (2.1)$$

Where V_x is the flow velocity (m/s), Q_x the volumetric flow rate (m^3/s), and D_x the diameter of the pipe (m).

By assuming an isokinetic condition between two flow systems, for example an extraction system and a fume collection system, you can then determine the isokinetic flow rate (equation 2.2)[16].

$$\frac{Q_n}{Q_p} = \frac{D_n^2}{D_p^2} \quad (2.2)$$

Where Q_n and Q_p are the volumetric flow rates of the sample pipe and extraction pipe respectively (m^3s^{-1}), and D_n and D_p are the diameters of the sample pipe and extraction pipe respectively.

Equation 2.2 shows that by altering the pipe diameters, and controlling the volumetric flow rates in both systems the isokinetic condition can be achieved.

2.4.2 Sample concentration

In addition to an isokinetic condition through which laser generated fume can pass, a method for collecting analytes from the flow must be used. As the gas phase material generated during laser processing may be small in volume, the corresponding concentration of the analytes is expected to be very low. Consequently it is necessary to choose an analysis technique capable of pre-concentrating the fume.

Here we have used solid phase microextraction as the analytes are progressively absorbed to the SPME fibre increasing their concentration. Solid phase microextraction is a method that can be employed where substances in vapour form or of low concentration are involved. SPME is simple, inexpensive and solvent free [19].

Solid Phase Microextraction works via a partition coefficient or distribution ratio of the analyte between a matrix and a coated silica fibre. The distribution of the analyte reaches equilibrium when a certain amount has been adsorbed by the fibre. Due to the concentration of the analyte on the fibre, mass resolution is maintained and minimum detection limits are improved [20].

Lee et al. [21] used a GC-MS system to study volatile organic compounds in workplace air. [21] The SPME needle was inserted directly into a polyvinyl fluoride bag called a Tedlar bag, through a septum. The needle was then removed after extraction for 15 minutes and the SPME fibre was directly exposed to 250°C for 5 minutes in the gas chromatography injector. Connected to the gas chromatograph (GC) was a mass spectrometer detector which scanned a mass range from m/z 35 to 280 amu. This set up involves the use of extra equipment such as gas tight syringes and the procurement of an SPME coated fibre with plunger function [21].

Before experimental use, the fibre must be conditioned at the recommended temperature [22] in the GC-MS inlet. This removes any substance adsorbed onto the fibre previously or during storage.

Thermal desorption tubes (Tenax Ta) were used to sample biological and environmental volatile organic compounds (VOCs) in the workplace [23] and also to

sample gas and vapours from IR irradiation of PVC [6]. The tubes were conditioned by passing through 100mL/min of nitrogen at 320°C and were proven to be stable for at least 30 days. To transport them, the tubes were capped and stored in an air-tight jar at 4°C[23]. In ambient workplace air, 26 VOCs were found in concentrations lower than 8mg/m³. Thermal desorption tubes are compatible with a wide range of chemicals and mass ranges, and can be used at different atmospheric concentrations [23]. The tubes can be input into a thermal desorption instrument coupled to a GC-MS for quick and simple identification of chemicals.

2.4.3 Sample transfer and Tedlar bag sampling

With an isokinetic condition achieved, a sample can then be collected. In order to analyse fumes from laser sintering of transparent oxides, gas will be collected via isokinetic extraction. There is a risk that the sample may have cooled down and condensed the further it flows from the laser interaction site. Therefore this method involves filling a polymer Tedlar bag, isokinetically (section 2.4.1). The Tedlar bag can then be introduced to an oven to volatilize and condensed vapour.

The Tedlar bag consists of a polymer bag with a sampling port containing a septum, the bag fills as gas is pumped in. Tedlar is the trade name for polyvinyl fluoride film developed in the 1960s. Tedlar film is tough yet flexible and retains its properties over a wide range of temperatures. Other advantages to Tedlar include low permeability to gases, good chemical inertness, good weathering resistance and low off-gassing.[24] The Tedlar foil is transparent to UV light and so should be kept out of sunlight to avoid disrupting the samples. Compounds commonly detected

already in the bags include: methylene chloride, toluene, acetone, ethanol, 2-propanol, phenol, and dimethylacetamide [24]. These can interfere with the fume analysis and should be accounted for.

Some substances may be absorbed by the bags with use so it is advised to consider the data quality objectives before reusing the bags, for example if low ppbv levels are expected [24]. In order to reduced potential contaminants from the bag itself, flushing with pure nitrogen or compressed air is recommended before use [25].

There are two methods used to sample with a Tedlar bag: sampling with a rotary vane pump and sampling with diaphragm pump. The diaphragm pump avoids contamination as the components which are in contact with the sample are sealed. The diaphragm pump used must have a small flow rate (0-5L/min) and a piece of tubing to fill the bag.

Tedlar bags are available with a single polypropylene fitting or dual stainless steel fittings so can be coupled to polymer and rubber tubing or metal pipes [26].

It is also possible to adsorb laser fume analytes directly onto an SPME fibre. Seneviratne et al. used laser adsorption with a mid IR laser to irradiate targets [27]. The sample was drawn into a heated tube suspended 1mm above the laser target. From this tube the analytes were captured on the SPME fibre, and then introduced to the GC injector [27]. This research states that combining mass spectrometry with SPME can detect small amounts of complex mixtures. This leads to a versatile active fume sampling approach which is also robust and cost effective. The only drawback of this system is the inability to separate the sample

before analysis [27]. Laser desorption sampling, collection of gas-phase products from laser-material coupling, was first demonstrated with a pulsed visible dye laser and an optical fibre inserted into a GC capillary column [27]. Seneviratne et. al. determined that an energy of 1.2mJ per pulse was sufficient to produce SPME detectable results [27]. They also found that less than 200ng of a substance, such as caffeine, deposited at the laser interaction site did not produce a detectable GC-MS signal. Therefore the sensitivity and detection limits of the GC-MS determine the minimum amount of material that can be identified. They calculated the capture efficiency to be 4% from the ratio of peak intensity of laser ablated substance to the peak intensity of the headspace analysis of the same analyte. If the capture efficiency is only 4%, it can therefore be deduced that 96% of the fume is released into the atmosphere or drawn into an extractor. A low capture efficiency indicates that a very sensitive technique is necessary, such as SPME which pre-concentrates the sample. The metal transfer line between the laser interaction site and the SPME fibre was held at 85°C by heating tape to avoid condensation of the vapour [27].

2.5 Particulate capture techniques

It has been determined that particulates produced by laser irradiation can be smaller than 100nm in size. Furthermore, particulates that are between 20-80nm can transpire through the lungs into the blood stream [9]. Schultz summarised several particulate capture methods utilising an air flow from an extraction unit. The methods include a hollow wand with 22.2mm internal diameter (ID) that was

situated very close to the laser interaction site and had a capture efficiency of 95% [9]. Also a device was developed that used open cell foam sandwiched between non-porous plastic which was connected to a 31.75mm (ID) pipe to the extractor. The capture efficiency of this method was 99.5% and had the advantage of a large surface area [9]. It was determined that the flow rate required to capture the fume produced was between 0.48-0.62m³/min [9]. To avoid re-entry of the laser plume to the manufacturing location, a HEPA filter is advised to collect 99.97% of particles 0.3 μ m in diameter or larger [9].

Mirzaee et. al. showed it was possible to capture airborne particles by pumping the air in the form of microscale bubbles through distilled water [28]. The device fabricated was called an impinger, and consisted of multiple 68x100 μ m gas inlets, 40 μ L of water, and a 2mm diameter gas outlet. The flow rate through the device was between 0-100mL/min. The experiment undertaken involved air containing polystyrene latex particles of 0.5, 1, and 2 μ m diameter. To measure the number of particles going into and leaving the device, a 200nm pore size membrane filter was used. From this the capture efficiency was calculated. The values are shown in table 2.1.

TABLE 2.1: Capture efficiency as a function of particle size and flow rate of a microimpinger. Data from [28].

Capture efficiency			
Particle size μ m	Flow rate mL/min		
	10	15	20
0.5	99.4%	95.4%	95.2%
1	94.2%	96.0%	95.2%
2	100%	99.7%	100%

The larger particles seem to migrate to the liquid more easily than smaller sizes, however it is interesting to note that the slowest flow rate does not determine the highest capture efficiency.

Palanco et. al. were able to capture gold particulates from laser ablation at fluences 10-100J/cm² on silicon witness plates. These witness plates were situated perpendicular to the gold sample and horizontal to the incoming laser. Two plates were used to determine the spatial distribution of the ablated particles. The silicon plates were imaged via scanning electron microscopy (SEM) after irradiation [29]. Similarly, Tillack et. al. [30] measured the distribution of condensate by atomic force spectroscopy on metallic coated silicon wafers with a roughness of approximately 4 Å. They determined that with an increase in laser intensity, the number density increased but the size of the particulates decreased [30].

2.6 Conclusion

In this chapter, literature concerned with irradiation via UV laser regimes was reported on. The photodegradation products are caused by direct bond scission due to the high photon energy of the incoming irradiation. This leads to small mass fragments that are in the gas phase. Irradiation by IR laser processes was also reviewed showing thermal decomposition products. These by-products were comprised of particulates, condensed material, and components that were similar to the effects of burning. Existing gas sampling techniques were described including isokinetic sampling, concentration, and capture of a sample. Also literature

involving the collection of particulates from an air flow was reviewed. The irradiation and laser cutting of polymeric materials was reviewed as there is a possibility of fume from polymers originating from two sources in this research. These are irradiation of the ink and substrate. The ITO ink in this research contains a polymer subcomponent. And future work is to include laser fume analysis of printed ITO ink on polymeric substrates, as they are ideal for flexible electronics.

From the above literature, SPME seems the most suitable method to collect and analyse a sample due to its suitability for low concentrations and its ability to pre-concentrate the analyte. Gas samples should be collected in a Tedlar bag which would be suitable for workplace sampling. Furthermore, particulates can be captured via filters (HEPA), bubbling through liquid, or via witness plates. Witness plates should be chosen as there are no limitations on the size of particle and flow rate of the system. Also witness plates are simple to visualise via SEM.

In summary, a system comprising of SPME analysis from sample collection in a Tedlar bag should be utilised. And witness plates should be situated around the laser interaction site to identify any particulates released from irradiation.

Materials

3.1 Introduction

The material of interest in this work was an ITO-based ink, comprised of three materials: ITO nanoparticles, a binder, and a solvent. This ink was developed and supplied, as a finished product, by the Leibniz Institute for New Materials (INM) in Germany [31]. Once deposited by spin coating, this ink is laser heated. Raising the temperature removes any unwanted organic material and increases the density of the structure so as to improve its electrical conductivity whilst retaining optical transparency. Therefore, an estimate of the potential laser-induced temperature rise required for decomposition could be obtained by looking at the characteristics of each component individually. The lasers used in this research were in the UV and IR spectrum. They include a RF:CO₂ laser (10.6 μm), a xenon chloride (XeCl) excimer laser (308 nm), and an argon fluoride (ArF) excimer laser (193 nm). In this chapter, measurements of the ITO nanoparticles, organic binder, and the solvent are presented. Particular emphasis is placed on their thermal decomposition temperatures as this will inform the possibility of laser generated fume. The substrates used and the thin film deposition technique is also introduced.

3.2 Nanoparticles

In order for the ink to be conductive, nanoparticles must be included. These consist of crystalline nanoparticles of ITO ($\text{In}_2\text{O}_3:\text{Sn}$, 8 mol% Sn) with an average size of 25 nm [32]. Puetz et. al. suggested a particle of $<30\text{nm}$ ensures low light scattering enabling use for transparent conducting materials [33].

The nanoparticles are dispersed in the binder and solvent. When heated, the polymer binder is removed and the distance between the nanoparticles reduces, increasing the conductivity of the film. Shown in figure 3.1 is the unirradiated surface of an ITO film which highlights the uniformity of the nanoparticles.

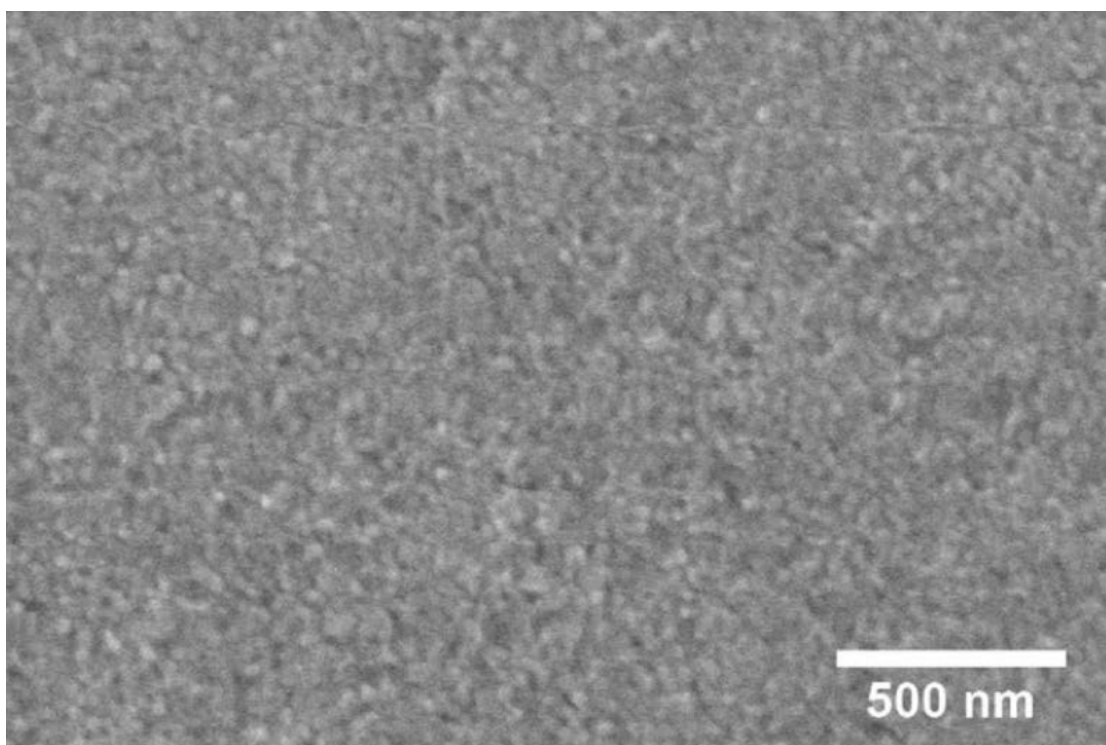


FIGURE 3.1: SEM image of an unirradiated ITO film showing the uniformity of the nanoparticles surrounded by MPTS binder. [32]

Table 3.1 shows the main characteristics of the ITO nanoparticles.

TABLE 3.1: Material characteristics of indium tin oxide nanoparticles distributed within the ITO ink [34].

Material characteristics	
Formula	$\text{In}_2\text{O}_3\cdot\text{Sn}$, 8 mol% Sn
Molecular weight	428.341 g/mol
CAS number	50926-11-9
Appearance	Yellow powder
Size	25nm average diameter

3.3 Binder

The 3-methacryloxypropyl-trimethoxysilane (MPTS) binder is a colourless viscous liquid that can be dropped onto the substrate to spin-coat. Table 3.2 outlines some characteristics of MPTS.

TABLE 3.2: Material characteristics of 3-methacryloxypropyl-trimethoxysilane (MPTS) used as a binder to incorporate all components of the ITO ink [35].

Material characteristics	
Formula	$\text{C}_{10}\text{H}_{20}\text{O}_5\text{Si}$
Molecular weight	248.35 g/mol
CAS number	2530-85-0
Appearance	Colourless liquid
Melting point	-19.99 C at $\approx 1,013.0$ hPa
Boiling point	190°C
Vapour pressure	0.023 hPa at 25°C

For the MPTS binder in air (Fig. 3.2), the thermogravimetric analysis (TGA) data shows that mass loss begins at $\approx 375^\circ\text{C}$. From the trace it can be seen that 50% of the MPTS thermally degrades by 500°C .

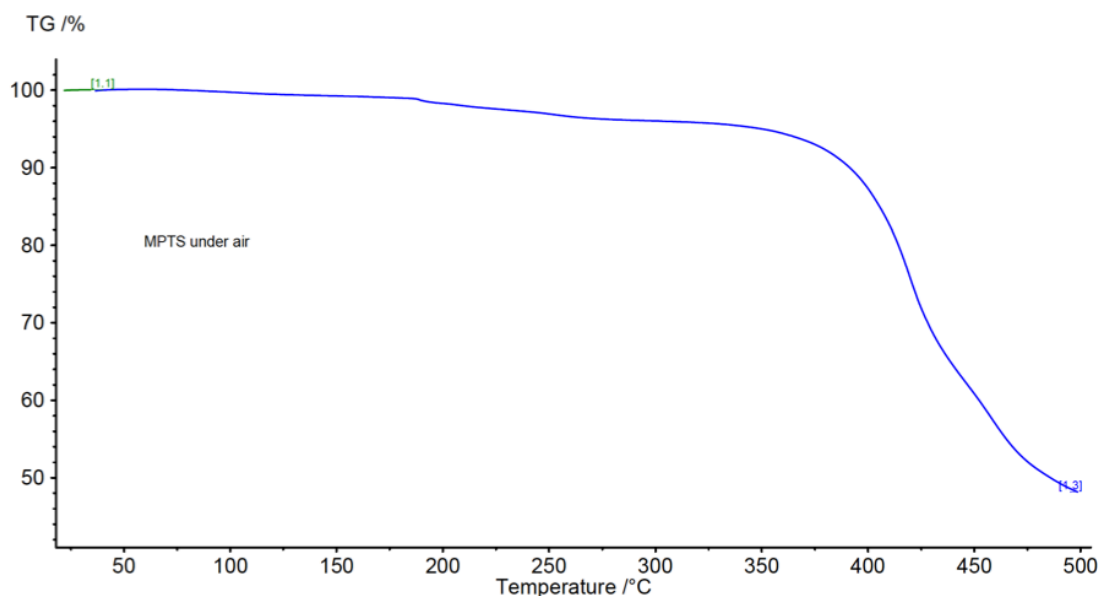


FIGURE 3.2: TGA trace for heating the MPTS binder in air. Decomposition of the material can be seen to occur for temperatures exceeding approximately 375°C.

In order to produce a fingerprint chromatogram for the MPTS binder, headspace analysis was performed. Firstly, 5ml of the MPTS binder was deposited via micro pipette into a headspace vial. An SPME fibre that had been conditioned at 270°C for 30 minutes was inserted through the vial septum and exposed. The fibre and vial assembly was then placed in an oven at 60°C for a 60 minute extraction and was then introduced to the GC-MS and analysed.

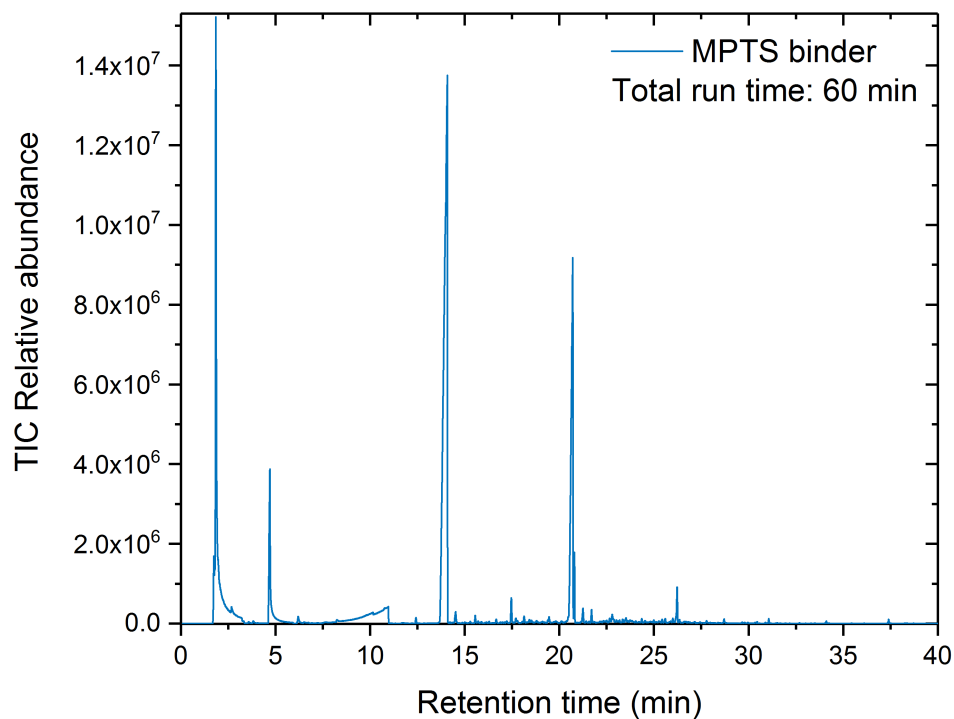


FIGURE 3.3: Chromatogram of MPTS binder extracted via SPME in an oven at 60°C for one hour.

Figure 3.3 is the fingerprint chromatogram for the MPTS binder. As well as the air peak at approximately 2.5 minutes, there are three significant peaks at 5, 14 and 21 minutes which are (2Z)-2-butenic acid methyl ester (CAS no. 4358-59-2), butyl methacrylate (CAS no. 97-88-1), and tributylamine (CAS no. 102-82-9) respectively.

3.4 Solvent

The role of the solvent in the ITO ink was to dilute the MPTS and nanoparticle mixture. Dilution was necessary for uniform deposition via spin coating. The solvent used was 2-isopropoxyethanol (IPE), the characteristics of which are outlined in table 3.3.

TABLE 3.3: Material characteristics of isopropoxyethanol used within the ITO ink. [36, 37].

Material characteristics	
Formula	$C_5H_{12}O_2$
Molecular weight	104.15 g/mol
CAS number	109-59-1
Appearance	Clear colourless liquid
Melting point	-89.99°C
Boiling point	42 - 44°C at 17 hPa
Vapour pressure	3.5 hPa at 20°C
Water content	0.06%/553.50ppm

Figure 3.4 shows that mass reduction of isopropoxyethanol during TGA occurs almost immediately as the temperature increases from 33°C. Observed is a 100% mass loss occurring by approximately 120°C. The sample size was 45.39 mg and the temperature ramp began at 25.0°C and increased by 5K/min to 350.0°C.

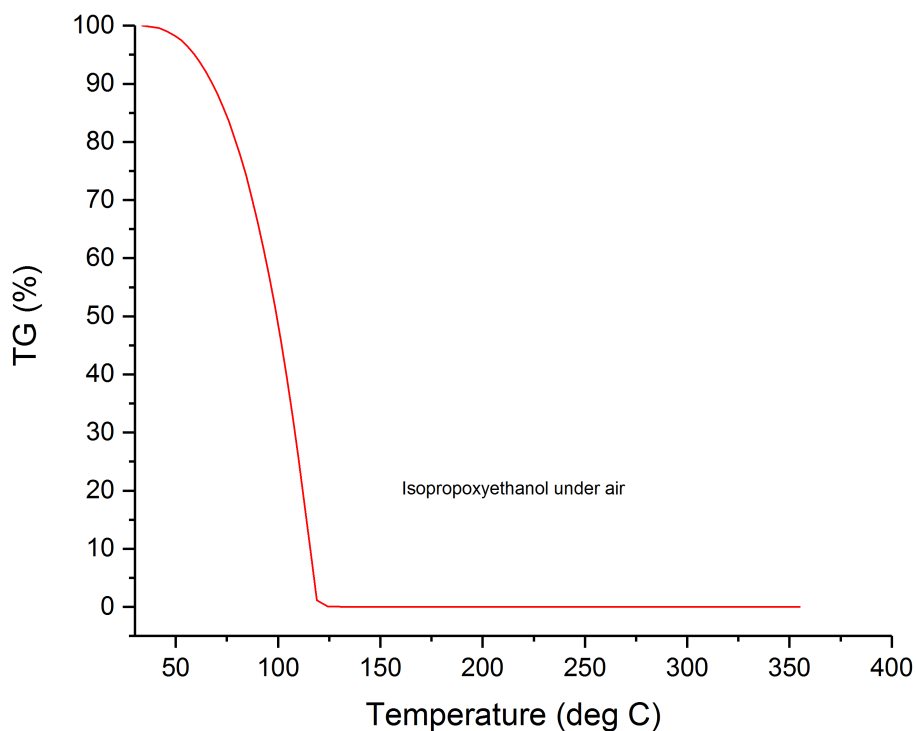


FIGURE 3.4: TGA trace for heating the isopropoxyethanol solvent in air. Evaporation of the material can be seen to occur for temperatures exceeding approximately 50°C.

3.5 Substrates

The substrate used was Borofloat-33 glass [38]. The chemical composition of Borofloat-33 is as follows: silicon dioxide (SiO_2) 81%, boron trioxide (B_2O_3) 13%, sodium oxide/potassium oxide ($\text{Na}_2\text{O}/\text{K}_2\text{O}$) 4%, aluminium oxide (Al_2O_3) 2% [38]. The dimensions of which were 50 x 50 x 2mm. For some experiments, smaller substrates were required. These samples were produced from larger sheets of glass that were cut with a diamond tipped glass cutter. Glass substrates were chosen as they're relevant to the display industry i.e. transparent in the visible spectrum.

Flexible polymers would be ideal for flexible electronics however difficulties occur under heat treatment. Since glass doesn't damage as easily, it was selected. A borosilicate glass is preferable due to its low coefficient of thermal expansion [38]. For this project's purpose, it is necessary to use a substrate that is completely transparent to visible light such as borosilicate glass, however this is not 100% transparent at UV and IR wavelengths. In figure 3.5 it is shown that the transmittance at 308nm is approximately 70% for a thickness of 2mm. It is necessary to consider the substrate when choosing the laser regime for laser processing as the transmittance of the substrate determines how much energy is absorbed. This can cause damage. If the substrate is damaged it is likely the conductivity of the film above will be compromised.

Borosilicate-33 can be cleaned with any commercially available glass cleaner [38], however the samples were kept stored from manufacture to laser processing and therefore unlikely to be contaminated.

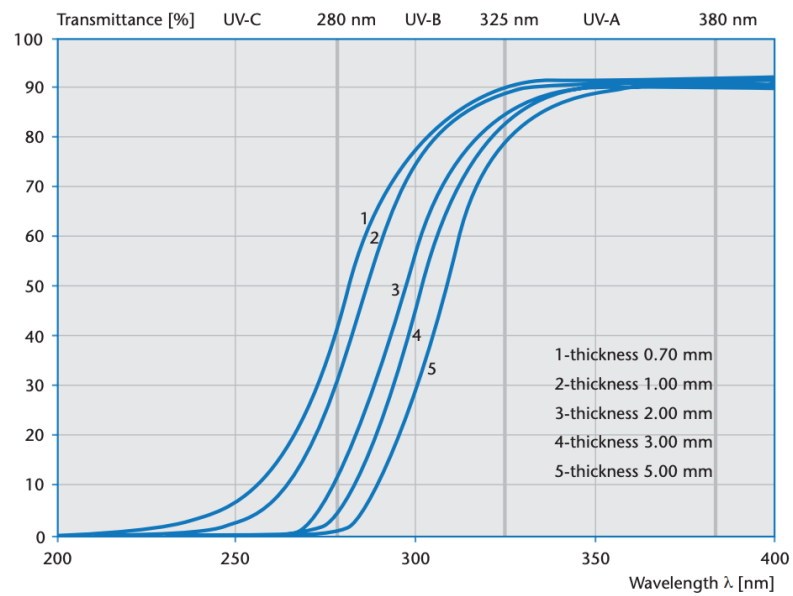


FIGURE 3.5: Borofloat-33 transmittance in the UV Range. The glass samples were 2mm thick and a wavelength of 308nm was used for laser processing of glass samples [38].

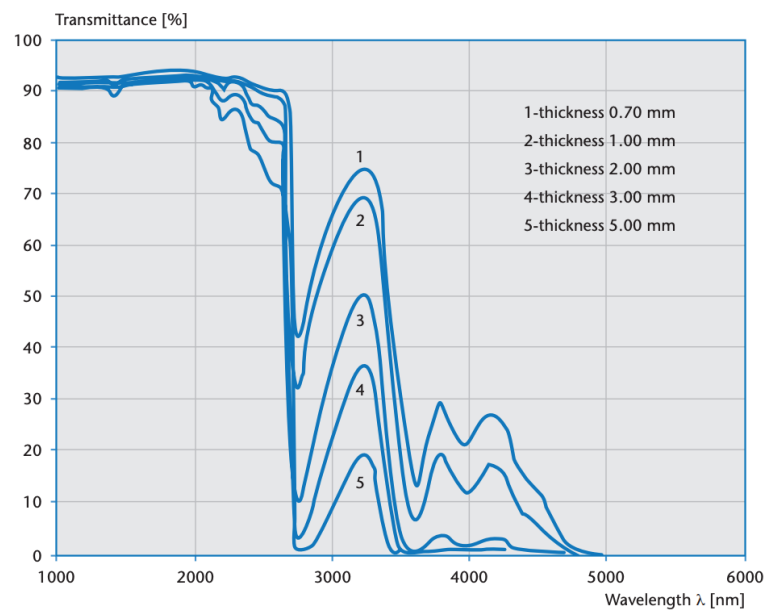


FIGURE 3.6: Borofloat-33 transmittance in the IR Range. The glass samples were 2mm thick and a wavelength of $10.6\mu\text{m}$ was used to laser process glass samples [38].

3.6 Ink

The ink comprised of three materials: ITO nanoparticles, a binder, and a solvent. The percentage composition is noted in table 3.4. This mixture of compounds was designed to create a printable ink that could be used in processes such as gravure and ink-jet printing. In order to predict what might happen when a sample undergoes laser-induced heating, thermogravimetric analysis was completed for the ITO ink. The TGA was run under air to simulate the laboratory process in future experiments. Although the heating rate of the TGA instrument is markedly different to the laser heating rate, it can act as a guide to whether a particular component of the ink is expected to become volatile during processing. Such an analysis is shown in figure 3.7 for the ITO-based ink in isopropoxyethanol solvent and with the MPTS binder.

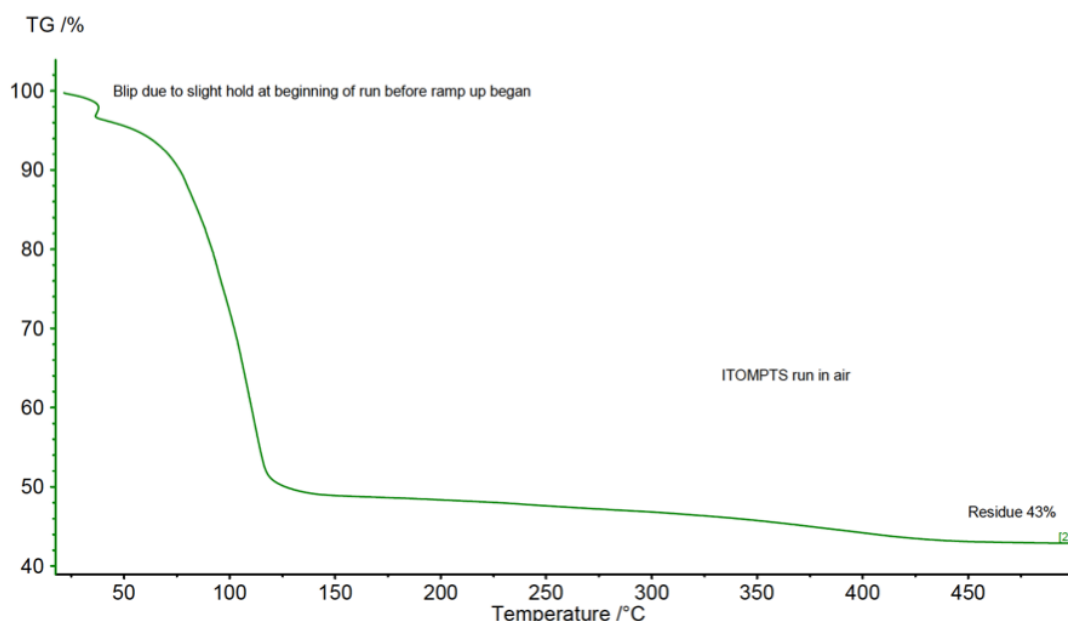


FIGURE 3.7: TGA trace for heating the ITO-based ink in air. The initial weight loss corresponds to the volatilisation of the isopropoxyethanol solvent. There is also a slight change in gradient between 350 and 400°C which is related to the MPTS binder.

A 72.19mg sample was used. The TGA temperature ramp started at 20°C, increased at a rate of 2K/min to 35°C, then increased by 5K/min to 500°C. Figure 3.7 shows that initially there is a dramatic loss in mass as the isopropoxyethanol solvent becomes volatile. Figure 3.4 shows that the isopropoxyethanol is removed up to 120°C of the temperature ramp which is also observed for the whole ink. This mass loss accounts for approximately 50% of the mass reduction at temperatures up to 500°C. In the 325 - 400°C range there is also a slight change in gradient. Figure 3.2 shows that MPTS degrades significantly at temperatures above 350°C which could therefore account for the mass loss observed of the ink.

In order to determine if the components of the ink break down individually in the same way as they do in the ink, comparisons of the mass loss of each component were undertaken. The table below (table 3.4) shows the percentage of the components present in the ink observed from TGA, versus the actual wt% of the components. The temperature ranges where the MPTS and IPE mass losses were observed were 325-450°C and 40-150°C respectively. These were used for the calculations in table 3.4.

TABLE 3.4: Analysis of figure 3.7 assuming the features are associated with the corresponding components of the ink.

	ITO	MPTS	IPE	Residue
Composition	40%	6.4%	53.6%	0%
TGA loss at 500°C individual components	n/a	50%	100%	0%
Predicted TGA loss	0%	3.2%	53.6%	40%
Ink TGA loss from figure 3.7	0%	3.07%	45.8%	43%

Table 3.4 shows that 8.06% of the ink is unaccounted for within the TGA of the components. The expected percentage of the MPTS and IPE in the ink differs from the actual value by 3.93% and 16.0% respectively. The value for residue of the ink is within experimental uncertainty. The two main features of figure 3.7 studied were the immediate mass loss attributed to IPE, and the smaller mass loss at 350°C attributed to MPTS. Since the difference in measured mass loss and mass of the components in the ink was small, the assumptions can be made with confidence. It is interesting to note that the MPTS is in good agreement whereas the IPE is less so. This could be due to the IPE being far more volatile and some mass may already have been lost when the sample was transferred to the crucible and then to the TGA instrument. This may account for the 7.8% mass discrepancy between the measured and known mass values.

3.7 Coating techniques

There are several deposition methods available for ITO inks on glass such as ink-jet printing, gravure printing, and spin coating. There are advantages to each printing method. Spin-coating is a quick and easy method to manufacture uniform coatings. Gravure printing is a quick way to achieve high-volume low-cost patterning [39]. Ink-jet printing is the best method to reduce wastage as only the amount of ink needed to create a printed pattern is used. Therefore, ultimately ink jet printing will be the preferred method to reduce the amount of ITO used as it is a finite resource as described in chapter 1.

3.7.1 Spin-coating

All of the samples used in this work were manufactured by spin-coating. The ITO ink samples were spin-coated and heat treated at 70°C for ten minutes by INM, and the MPTS/isopropoxyethanol films were manufactured in Hull. The spin coater used for these films was a Laurell WS-650. In preparation, the 50mm square glass substrates (Borofloat-33) were cleaned with isopropanol solvent to removed dust and fingerprints. The samples were spin coated within a fume cupboard as the chemicals used were expected to become volatile. Once dry, the substrates were secured to the suction plate of the spin coater by a vacuum. The glass was then rotated at 10000 RPM for 60s, whilst 100 μ L of MPTS was added immediately via a micropipette. Previous tests showed that a rotational speed of at least 10000 RPM was required for an even coating. For amounts of MPTS larger than 100 μ m there was a non-uniform distribution of material. Isopropoxyethanol was subsequently dropped onto the MPTS and substrate to encourage spreading and a uniform coating of the glass. When the samples were baked after deposition, the MPTS appeared to coalesce and form a non-uniform coating. Therefore, the samples were left in the fume cupboard at room temperature for 60 minutes before irradiation with a laser.

3.8 Conclusion

As discussed above the materials used in this project have varying properties. Thermal analysis of the ITO ink showed that isopropoxyethanol was removed

from the ink up to 120°C, and thermal degradation of the MPTS binder occurred at temperatures exceeding 375°C. A fingerprint chromatogram was produced of the MPTS binder in order to compare with chromatograms of laser fume in future experiments. Characteristics of the ITO nanoparticles were discussed and the uniformity of the films with 25nm particles was shown in figure 3.1. Finally the coating techniques used to manufacture the ITO films were discussed.

During processing, if the laser heats the film to 350°C, we would expect to get decomposition products of MPTS in the fume. The softening point of the borofloat substrate is 820°C[40]. The chromatograms in chapters 4 and 5 and the TGA data above, show that below the melting point of glass fume is still produced. The temperature that the film and substrate reach is not known when irradiated with the laser, however if we work below the damage threshold of the glass, gas phase products are still expected to be measured.

Static Sampling

4.1 Introduction

In this chapter the process of identifying fume products collected by static sampling of laser fume is developed. Static sampling encompasses closed cell systems or experiments with no extraction. This means that fume created via laser processing is not transported in an ambient gas flow and is therefore accumulated for analysis. Firstly, the nomenclature involved in fume analysis will be discussed including sampling methods and fume products. The development of the GC-MS method used for the identification of gaseous fume products will be illustrated. Then the static method for sampling laser fume will be explained and the GC-MS results for static sampling of RF:CO₂ 10.6 μ m laser irradiation of MPTS and ITO based spin-coated films will be shown and discussed.

4.1.1 Background to the experimental techniques

To account for the possibility of condensed phase material and also to concentrate the analytes in preparation for GC-MS, the technique of solid-phase microextraction (SPME) was used [41]. A schematic of the sampling to analysis process is shown in figure 4.1.

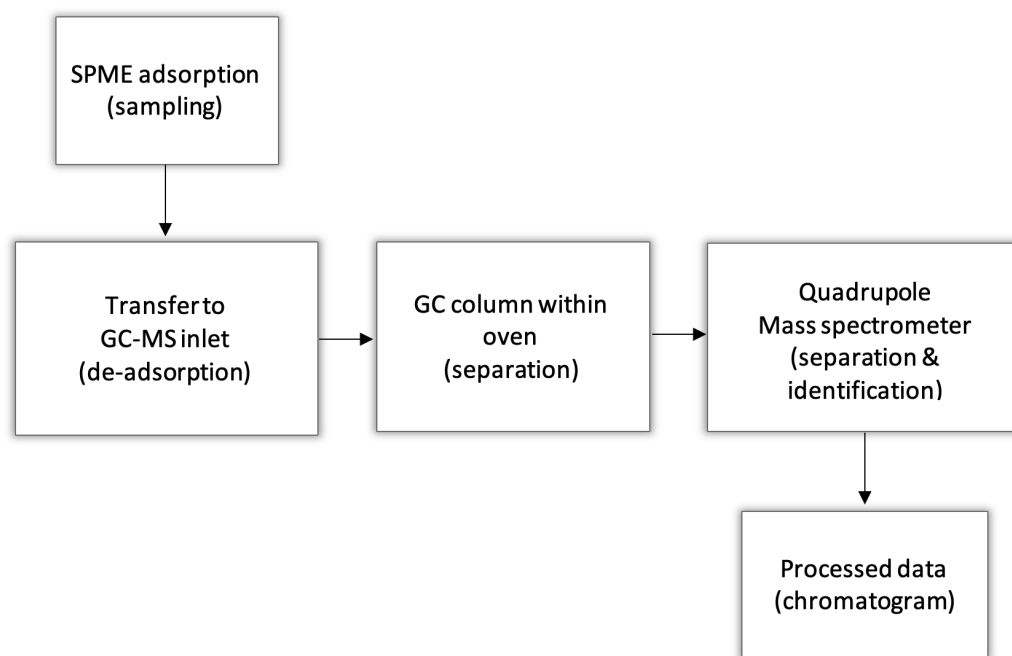


FIGURE 4.1: Process diagram from sampling to data analysis.

Substances that contain volatile organic analytes in the gaseous phase can be sampled via SPME. Solid-phase microextraction is a technique using a flexible fused silica fibre covered in an adsorbent polymer coating. Analytes from the sample adsorb to the fibre if they fulfill certain characteristics, for example compounds that are non-polar will show a higher affinity for a coating such as polydimethylsiloxane which is also non-polar [42]. This research used a 2cm, 50/30 μ m film thickness, divinylbenzene/carboxen/polydimethylsiloxane (DVB/CAR/PDMS) coated fibre mounted on a 23 gauge needle [43]. The fibre used in this study was chosen due to having the largest applicable mass range to sample unknown molecules (40-275g/mol)[44]. When injected into the heated inlet port of a GC-MS instrument, the analytes de-adsorb into the carrier gas and flow through the system to be analysed. This leaves the SPME fibre free from adsorbents and ready for further

use. This is known as a conditioned fibre. The SPME fibre is conditioned until there is no analyte signal on the GC-MS. The fibre is then removed from the GC inlet port and used to adsorb laser generated fume samples following which, it's re-entered into the GC-MS for analysis of the fume sample.

In the Agilent 6890+ GC used, the vapourised sample is carried by an inert carrier gas helium, and injected into the chromatographic column. Analytes enter the Rxi-5ms GC column which consists of a long tube of fused silica of at least 10m. The length of the column used, which affects the speed of analysis and resolution of peaks, was not recorded, but the shortest Rxi-5ms column available to buy is 10m. The fused silica tube contains the stationary phase of 5% diphenyl to 95% dimethyl polysiloxane and has an external protective polyimide cladding [45, 46]. The carrier gas enables transport of the mobile phase through the column but does not interact with the stationary phase or the molecules of the analyte [45]. The separation of the sample occurs as a result of a differential distribution between the mobile and stationary phases in the column, and the fraction of time the sample resides in the mobile phase [45]. Molecules strongly retained by the stationary phase will move slowly in the flow of the mobile phase and are observed as a peak at a later retention time on the chromatogram. On the other hand, molecules weakly held by the stationary phase move quicker in the mobile phase and appear as a peak at a shorter retention time. Also as the sample moves through the column, it dilutes. This means the volume of gas in the column containing the analytes increases as the mobile phase moves through the column and band or peak spreading occurs on the chromatogram [45]. The flow rate of the mobile

phase through the column is low enough to be fed directly into the ionization chamber of the mass spectrometer (MS) [45].

Analytes from the sample are identified by mass spectrometry. The MS produces ions and separates them by their mass to charge ratio (m/z). Since most ions in the spectrometer have a positive or negative charge of 1, their m/z value is often equivalent to their mass number [45]. A small amount of the sample is injected into the MS inlet which introduces the sample to the ion source which forms gaseous ions by bombardment with electrons [47]. Electron ionization forms positive ions since the charged beam of electrons approaches the sample molecules close enough for them to lose electrons by electrostatic repulsion [45]. The sample is then accelerated into the mass analyser whose role is to separate out the analyte ions by their m/z ratio. A detector then converts the separated stream of ions into an electrical signal from which the MS software produces a mass spectrum. The MS process from the ion source to the detector must be completed under vacuum in order to extend the mean free path of the ions. The MS used in this research, an Agilent 5973N, includes a monolithic hyperbolic quadrupole mass analyser and an electron multiplier detector [47].

The quadrupole consists of four parallel hyperbolic (in cross-section) rods which act as electrodes. Opposing rods are connected to the negative terminal of a variable direct current (DC) source, and the other opposing rods connected to the positive terminal. Also, variable alternating current (AC) voltages, which are 180° out of phase, are applied to both sets of rods. Consider a positive ion that enters the quadrupole. If the ion is heavy it is harder to deflect from a stable

trajectory and will be less affected by the AC voltage and more so by the DC voltage. Between the two positively charged rods, a heavy ion is more likely to have a stable trajectory, be less affected by the AC voltage and consequently pass through the quadrupole and onto the detector. Therefore the pair of positive rods act as a high-pass filter for ions with a large m/z ratio. On the other hand, without the presence of an AC field, all positive ions will be drawn to the pair of negatively charged rods and will be neutralised. However with the application of the AC voltage, low mass ions will be diverted and the movement will be negated, leaving the low m/z ions to travel through the quadrupole. The pair of negative rods act as a low-pass filter for the low m/z ratio ions. For each set of DC and AC voltages there is a limited range of m/z ratio values that travel through the quadrupole unaffected. Once the ion beam exits the quadrupole, it is accelerated to several thousand electron volts in order to have sufficient kinetic energy to liberate secondary electrons from the first part of the detector. The electron multiplier is in the shape of a horn made of a low conductivity material over which a voltage gradient is applied. Ions from the accelerated beam eject electrons from where they strike. These electrons are then accelerated to higher energies further down the horn and can liberate further secondary electrons. At the end of the electron multiplier a current gain of at least 10^5 is achieved [45]. As an MS scan progresses the filtered m/z range is increased in value by varying the AC and DC voltages in the quadrupole at a constant ratio. This results in a mass spectrum of peaks ranging from low to high m/z ratio values, which have originated from the vapourised sample and are identified by the MS software. The resolution of the MS is set to 1amu meaning a MS can resolve analytes of masses

differing by 1 atomic mass unit [45]. By previously separating the sample by GC, the resolution can be further improved as each section of the ion beam which enters the quadrupole will only consist of discrete values of the m/z ratio.

During a GC experiment, the MS scans the masses repeatedly. A quadrupole mass analyser is useful for this purpose as their scan times can be less than 100ms. During a GC-MS run, many mass spectra are recorded throughout the chromatographic process. In this research a mass spectra was recorded every three tenths of a second. This data can be interpreted in three ways. Firstly, the ion abundances for each spectra can be plotted as a function of retention time to create a total-ion chromatogram. Secondly, the mass spectra at a particular time during the GC run can be displayed showing only the analytes which are detected at that point. Finally, the ion abundance for a specific m/z value can be plotted as a function of retention time and a selected-ion or ion-extraction chromatogram produced [45]. The ability of GC-MS instruments to analyse mixtures in this way makes it useful in identifying unknown laser fume which may consist of analytes with widely ranging, or very similar, m/z values.

4.2 Optimisation of the GC-MS method

The headspace data for MPTS in section 3.3 indicated GC-MS might not be sensitive enough to determine individual fume constituents, therefore optimisation of the GCMS method was completed through extraction and identification of organic solvent fume.

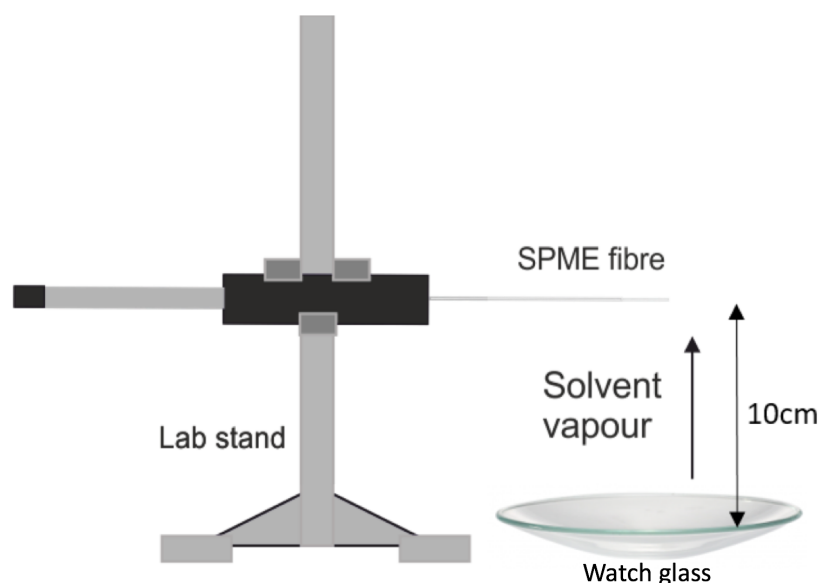


FIGURE 4.2: Direct exposure of a conditioned SPME fibre above a watch glass containing approximately 2ml of HPLC methanol. This method was intended to increase the relative abundance of methanol adsorbed and hence allow identification via GC-MS.

This involved directly exposing a conditioned SPME fibre to solvent fume above approximately 2ml of high-performance liquid chromatography (HPLC) standard methanol contained in a watch glass (see figure 4.2). This was expected to increase the relative abundance of methanol captured on the fibre and therefore increase the possibility of solvent identification via GC-MS analysis. This was also a test to make certain that the DVB/CAR/PDMS SPME fibre is suitable for methanol adsorption since the molar mass of methanol is 32.04g/mol which is slightly below the fibre mass range of 40-275g/mol [44]. Also mass fragments of this size are possible from laser-induced decomposition of isopropoxyethanol used in the manufacture of the ITO films.

The conditioned fibre was exposed to the methanol vapour for 5 minutes at an ambient temperature of 20°C. The SPME fibre was subsequently transferred to the

injection port of the GC-MS (Agilent 5973N mass selective detector with Agilent 6890+ GC, Rxi-5ms column, splitless) and re-heated in a 1mL/min flow of helium carrier gas. Using NIST libraries (Rev.D.04.00, October 2002), no methanol peaks were identified in the resultant chromatogram.

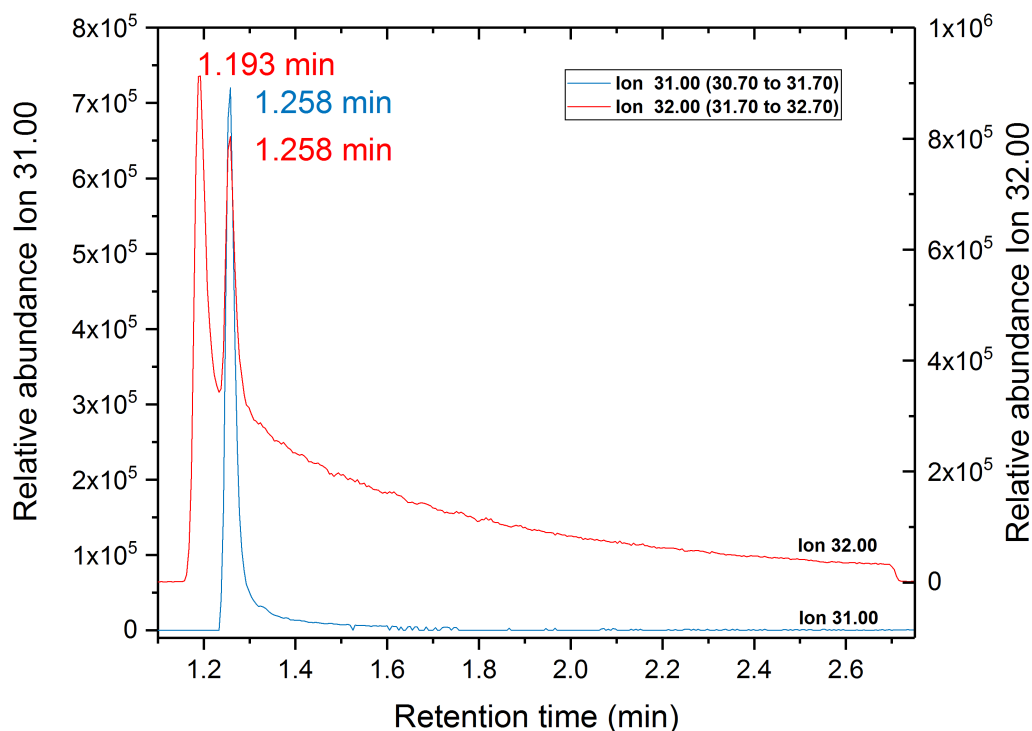


FIGURE 4.3: Ion extraction chromatogram of 31g/mol and 32g/mol molecular weights identifying the presence of methanol in the sample adsorbed to the SPME fibre. The method duration was 40 minutes with a flow rate of 1mL/min. The peak separation is 0.065 minutes. Ion values of 31.00 and 32.00 were both plotted to show whole methanol ions and also to account for methanol with a hydrogen removed which can occur in the GC-MS.

However, the presence of methanol was found with an ion extraction chromatogram (figure 4.3), from which a peak separation of 0.065 minutes retention time between the air peak and methanol peak was measured between the two maximum y-axis values. Methanol was successfully identified which was previously masked by the air peak which spans between 1 and 2.5 minutes retention time. In order to improve

identification of solvents, further separation of these peaks was desirable. In order for this to be achieved the flow rate of the carrier gas through the system was halved to 0.5mL/min effectively doubling the run duration and spreading out the retention times. The starting temperature of the GC oven was 40°C and this was kept constant for 20 minutes, thereafter the temperature was increased 5°C/min until 220°C, where it was held for another 20 minutes. The duration of the method was increased to 60 minutes to account for the lengthened retention times. Direct exposure of the conditioned fibre to methanol vapour was then repeated and the retention times of interest plotted (figure 4.4).

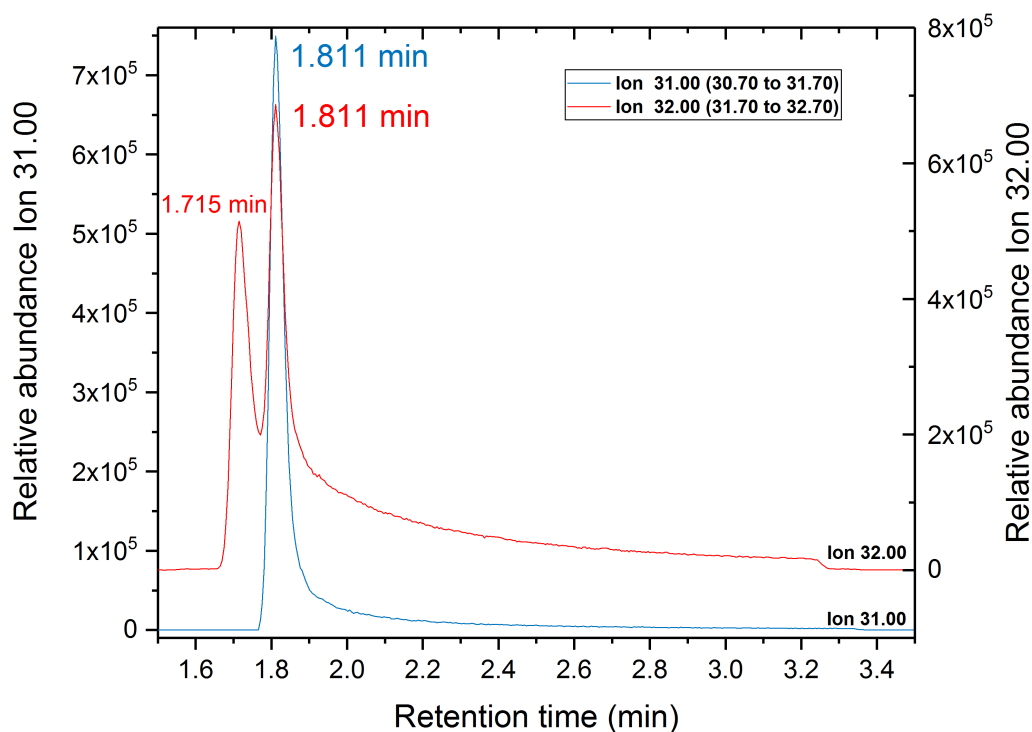


FIGURE 4.4: Ion extraction chromatogram of 31g/mol and 32g/mol molecular weights following reduction of GC-MS flow rate to 0.5mL/min. The peak separation is shown to be 0.096 minutes a 47% increase to previously (fig. 4.3). The total run time was 60 minutes but only the retention times of interest are shown.

An increased peak separation of 0.096 minutes was achieved and one more iteration of the GC-MS method was proposed. The oven starting temperature was reduced by 5°C to 35°C. The aim of decreasing the starting temperature of the oven ramp was to reduce the mass range of molecules that have sufficient vapour pressure at that temperature to desorb and enter the GC column. Analytes with the lowest mass are generally the most volatile and analytes will boil off when their vapour pressure equals ambient pressure. Reducing the mass range entering the column will further separate the peaks identified by the mass spectrometer. Direct exposure of the conditioned fibre was then repeated in order to compare the difference in chromatograms (figure 4.5).

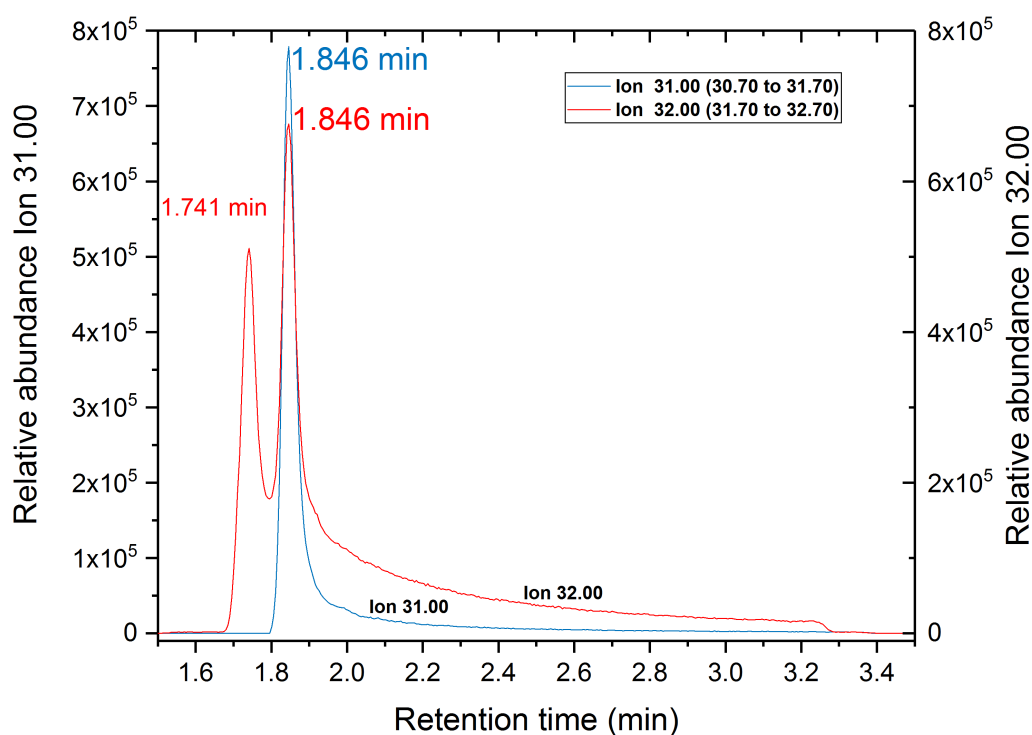


FIGURE 4.5: Ion extraction chromatogram of 31g/mol and 32g/mol molecular weights following the reduction of oven starting temperature to 35°C. A peak separation of 0.105 minutes was achieved, a 9.4% increase on the previous iteration.

Figure 4.5 shows that a further separation between the air and methanol peak was achieved. The 9.4% increase on the previous method shows that a reduced starting temperature has improved the identification of low mass organic solvent fume via SPME analysis and will improve the identification of unknown fume products in the following experiments.

4.3 Direct chamber sampling

With the GC-MS analysis process outlined in section 4.2, investigations of the suitability of the system for identifying laser generated fume were then conducted. In order to increase the concentration and reduce the distance travelled by the fume, the SPME fibre was injected directly into the laser processing chamber through a septum, as shown in figure 4.6.

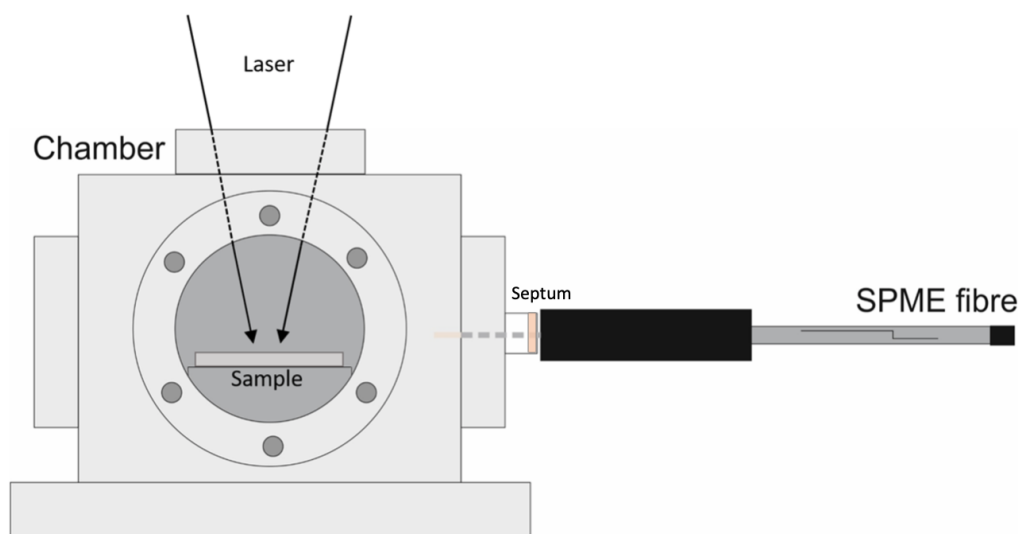


FIGURE 4.6: Drawing of the experimental set up with the conditioned SPME fibre inserted directly into the chamber via a septum.

Due to the thermal analysis shown in section 3.3, thermal degradation of the binder under laser treatment was expected if the laser-induced temperature is in excess of 375°C. The thermal analysis also indicated removal of the isopropoxyethanol solvent between 40°C and 120°C. To test this hypothesis, a thick coating of MPTS in isopropoxyethanol was prepared by spin-coating onto borosilicate glass, forming an uneven coverage that ranged from bare areas to $\approx 0.5\text{mm}$ thick.

As can be seen in figure 4.6, the beam size at the window limits how far the chamber can be translated, and this in turn limited the irradiated area to 2.5cm by 3.2cm. The sample was irradiated (figure 4.7) with the continuous wave RF:CO₂ laser, with a beam diameter of 550 μm (minimum beam size) in a rectangular spiral starting close to the centre of that area. The laser was set to pulse mode with a repetition rate of 1kHz and 350 μs pulse width. The beam overlap was 50% with a laser power of 7W.

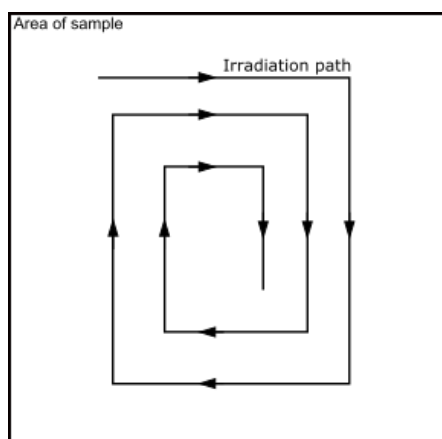


FIGURE 4.7: Schematic of the irradiation scheme concept. The irradiation path was created by programming an x-y translational stage with G-code, to move the sample within the chamber through a configured coordinate sequence.

The SPME fibre was exposed to the fume both during the laser irradiation as the fume was being generated, and for sometime afterwards as it was left exposed

inside the chamber. After approximately 15 minutes of irradiation the exposed fibre and chamber were transported to the GC-MS instrument. The SPME fibre was retracted into its housing, withdrawn from the septum and injected directly into the GC-MS inlet for analysis within 10 minutes of irradiation.

4.4 Results

Chromatograms were recorded using the optimised temperature ramping scheme described in section 4.2. Isopropoxyethanol was detected by GC-MS in its whole form, and a thermal fragment of MPTS was detected and identified as butyl methacrylate. Fragments were expected due to laser-induced heating of the sample as well as GC-MS inlet temperature of 250°C. Figure 4.8 shows that the isopropoxyethanol and butyl methacrylate peaks are far in excess of the air peak and are easily distinguishable. It was expected that both analytes would adsorb on to the fibre as they have masses of 104.15g/mol and 142.20g/mol respectively, which is within the mass range of the DVB/CAR/PDMS SPME fibre used (40-275g/mol).

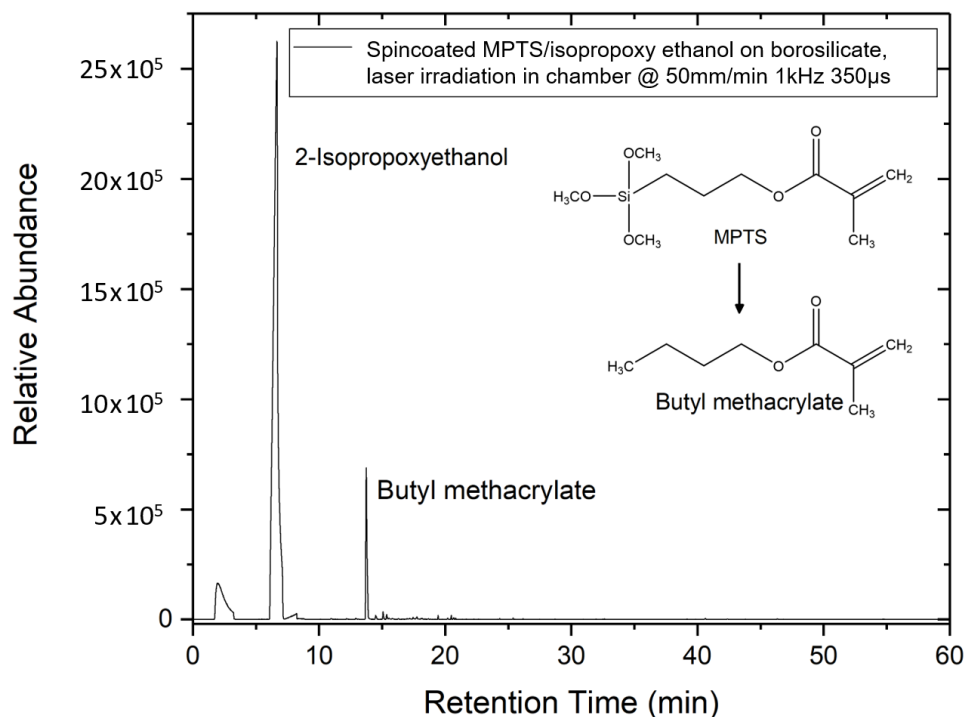


FIGURE 4.8: Chromatogram of borosilicate glass coated in MPTS with isopropoxyethanol solvent irradiated with the RF:CO₂ laser and the fume collected directly onto the SPME fibre in the chamber. The presence of butyl methacrylate [48], a methacrylate monomer, is shown which is a thermal decomposition product of MPTS [49]. It involves the separation of the silicon and three OCH₃ groups and replacement with a CH₃ group. This reaction is explained by Si-C bonds having a lower bond energy than C-C bonds which are therefore weaker [49].

Following the detection of thermal degradation products from irradiation in a cell of a spin-coated binder and solvent, an ITO printed structure was irradiated using the same laser parameters and irradiation method.

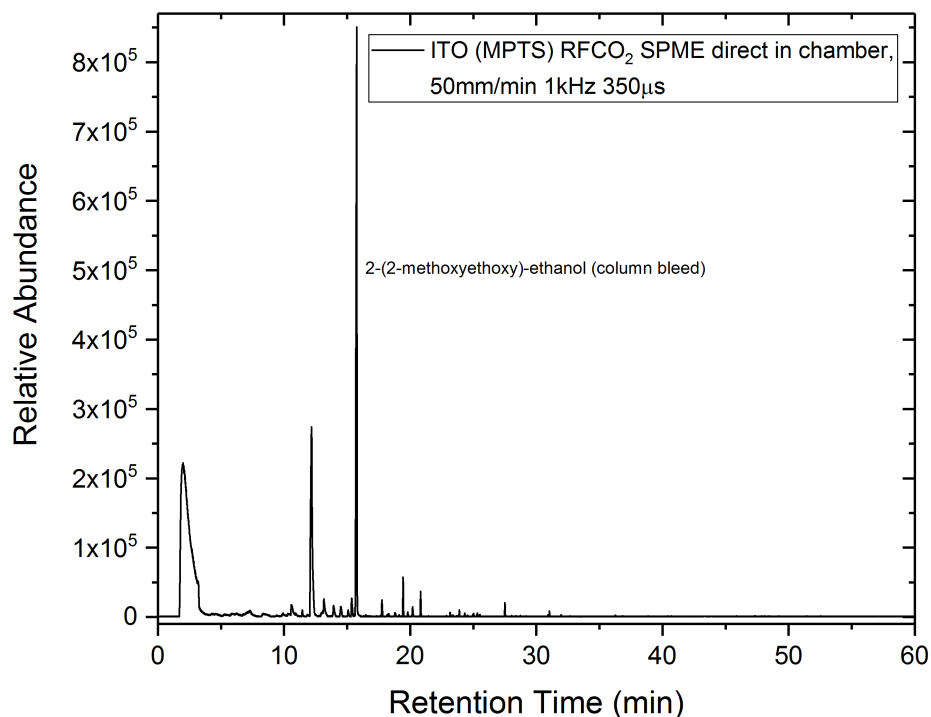


FIGURE 4.9: Chromatogram of spin-coated MPTS based ITO thin film with RF:CO₂ laser and the fume collected directly onto the SPME fibre in the chamber. No conclusive fume peaks are observed and the main peak identified is most likely column bleed. Column bleed is when the stationary phase contained in the column of the GC-MS leaks into the mass spectrometer, producing regular peaks of similar intensity (see decamethyl-cyclopentasiloxane peak at 19.4 min).

Figure 4.9 shows no conclusive fume peaks for the irradiation of an ITO printed structure in the chamber. This was the printed sample that was pre-dried by INM. The only peaks present represent air and column bleed, where the stationary phase of the the GC column leaks into the detector. The only peaks resolved are located at 2.007 (air), 2.097 (ethanol), 12.18 (col. bleed), 15.763 (col. bleed), 19.439 (col. bleed) minutes.

4.5 Discussion

Figure 4.8 shows thermal fragments from the sample, however, these have been produced using a laser regime that is above the damage threshold of the printed material and also on a spin-coated sample prepared with much larger amounts of binder and solvent. The comparatively large size of the peaks to the air peaks may be because the environment is more static and there is more time for fume molecules to adsorb on the fibre, or, that in a closed cell there is a fixed volume and consequently a higher concentration of fume.

The industrial purpose of laser irradiation of the ink is to increase the conductivity. Other researchers have shown this is predominantly through the removal of the MPTS binder [32]. If we increase the laser irradiation to the point where we remove the ink, then we have generated the worst case scenario of the maximum amount of fume and products that could be released in manufacture.

The vapour pressure of isopropoxyethanol at 20°C is 3.5hPa [36]. Laser heating will increase the vapour pressure so we would expect to find it in the analysis unless thermal degradation had occurred, which would happen at approximately 100°C as shown by the TGA in chapter 3. Despite the GC-MS injector being held at 250°C, isopropoxyethanol was still found in its whole form (figure 4.8).

The data in this chapter is not sufficient to quantify the success of the static sampling method, or conclude that laser heating leads to a higher relative abundance of alcohols identified during GC-MS. Future work should include a comparison of ion exchange chromatograms, such as those in figure 4.5, methanol sampled inside

the chamber with no laser irradiation, and methanol sampled inside the chamber under IR laser irradiation. This would show if laser heating had a significant effect on vapour pressure and whether that effect is larger than vapour being SPME sampled in a closed system.

Both figure 4.8 and figure 4.9 have a similar size and shape of air peak situated within the first 5 minutes retention time. This shows that SPME sampling reflects a consistent environment inside the chamber. Each time a spin-coated sample is placed inside the chamber and closed, there is the same volume and pressure of laboratory air contained in the chamber. As the chamber is airtight, no more air can enter after fume generation has started which explains why both air peaks are similar.

The amount of material prepared on the substrates may have contributed to the amount of fume produced. The spin-coated MPTS sample had a thickness of the order of hundreds of microns whereas the ITO thin film sample was 400nm thick [32]. Samples prepared by INM were dried at 70°C for 10 minutes and later irradiated at Hull. The spin-coated films were attempted to be dried but resulted in non-uniform thickness so they were irradiated wet. The only difference expected between irradiation of wet as opposed to dry spin-coated samples was a higher relative abundance of isopropoxyethanol measured in the chromatograms.

4.6 Conclusions

In this chapter, the GC-MS method was improved in order to increase the resolution in the low mass region. This is the first five minutes where the volatile solvents from the sample have already been removed from the fibre and travelled through the column. Direct sampling of a known chemical, methanol, was completed in order to observe the effect of varying the GC-MS parameters to give greater separation of the signal peaks on the chromatograms. From an original peak separation of 0.065 min, the GC-MS flow rate was halved which increased the separation to 0.096 min but doubled the run time. The GC-MS oven starting temperature was lowered to 35°C further increasing the peak separation to 0.105 minutes and improving the identification of analytes in future measurements.

Although useful to see the validation of the SPME sampling technique via the thermal degradation products in the chamber in the laboratory, due to lack of extraction this method is not analogous to large scale production since it is in a closed chamber. Although it is likely that the direct chamber sampling method increased the concentration of laser fume surrounding the SPME fibre, increasing the number of analytes adsorbed, and therefore the relative abundance of substances via GC-MS, this method is not the most relevant to laser fume in the workplace. Therefore a dynamic sampling system where fume is collected and analysed from an extraction flow was developed and is discussed in the next chapter.

Dynamic Sampling

5.1 Introduction

This chapter extends the work from chapter 4 by introducing flow into the system. The intention is to better mimic the real conditions of industrial fume sampling. This chapter covers the development of SPME analysis of laser fume from an extraction flow which we term dynamic sampling. Firstly, a technique to sample laser fume after irradiation from a carrier gas flow was developed. This involved collecting fume generated by laser irradiation in a chamber, followed by drawing it past an exposed SPME fibre. Secondly, a technique to sample laser fume from an air flow during irradiation was tested. Thirdly, an isokinetic system was designed to sample fume with content the same as that experienced by an extraction system and to collect the fume for analysis after irradiation. Contaminants found in this system resulted in changes in the choice of materials used that will be described later. Finally, a technique to sample particulates from a gas flow was used.

The research running parallel to this work was to determine which laser treatment improved the electrical conductivity of the material, and therefore informed the choice of lasers used for fume analysis. The choice of both UV and IR lasers for fume analysis was to determine the distinction, if any, between the fume from

photochemical and photothermal mechanisms. Results will be discussed for irradiation with the RF:CO₂ laser (10.6 μ m), XeCl (308nm), and ArF (193nm) lasers with regards to particulates and gaseous output from laser-material interactions.

5.2 Chamber cross-flow sampling

It has been shown by Chinthaka A. Seneviratne et al. that it is possible to perform SPME extraction on a gas phase sample moving past the fibre in a T-shaped connector [27]. This method was adapted to use a cross piece with an additional pressure gauge for the chamber in which the fume was collected, as shown in figure 5.1. This method follows on from use of the chamber in chapter 4.

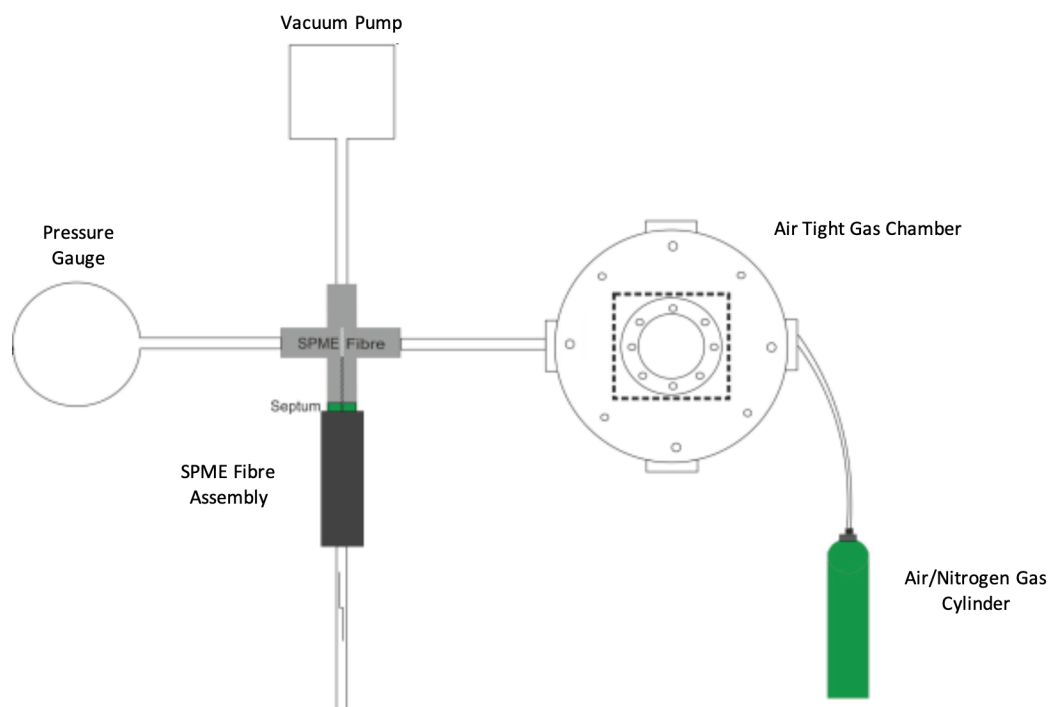


FIGURE 5.1: Schematic diagram of the cross-flow technique adapted from [27]. In the centre is a cross-shaped pipe connector with a septum in one port. The SPME fibre is extended past the septum, and fume from laser processing flows past from the air tight gas chamber. The third port connects to a vacuum pump used for controlling flow past the fibre and backfilling the chamber with nitrogen or compressed air, within the safety limits of the chamber windows. The fourth port connects to a pressure gauge which indicates the pressure within the chamber which can be compared with the maximum and minimum pressures of the NaCl windows (0.6-1.3 bar) and is also used for balancing flows.

A NaCl window was chosen for the chamber as salt is transparent to IR radiation, and the RF:CO₂ laser beam can pass through to irradiate the sample within. The salt windows available were not thick enough to completely evacuate the chamber without fracturing therefore it was decided to induce a flow of the fume past the SPME fibre by flushing with bottled (clean) air.

The test material was irradiated in the chamber as shown in figure 4.6. However, in this configuration, the fume is swept past the SPME by back-filling the chamber with clean air whilst the pump induces gas flow through the T-shaped connector.

The literature example was a dynamic sample, meaning the SPME fibre adsorbs analytes from a moving flow. By first irradiating the printed sample within a static atmosphere in the chamber, it was possible to control the flow rate past the fibre and therefore the time available for analytes to adsorb to the fibre. The flow was controlled by opening or closing the chamber valve to increase or decrease the flow velocity respectively.

Issues occurred with breaking fibres and bent housing due to insertion through the septum. Therefore the procedure was developed in accordance with Sigma Aldrich advice [50]. It is possible to change the length of the needle containing the fibre (fibre housing needle) that protrudes from the fibre holder. This is to allow for varying SPME GCMS inlet ports and experimental set-ups. The fibre housing needle is not rigid and therefore, the further it is extended from the fibre holder, the higher the risk of the needle flexing enough to damage the fibre within. The length of the fibre housing needle was reduced before penetration through the septum, and the range exposed, increased after the needle was securely pushed through the cross-section of the septum. When the desired extended range was reached, the 2cm SPME fibre contained within the housing needle was then exposed [43]. Improved septa were also obtained with a needle guide in the centre.

5.2.1 XeCl laser irradiation

The chamber cross-flow system shown in figure 5.1 was used to irradiate a spin-coated ITO ink sample on borosilicate dried at 70°C in an oven by INM. Due to the XeCl laser used, the windows used in the chamber were fused silica. Fused silica is

transparent to irradiation at 308nm. The spincoated ITO sample on borosilicate glass was placed in the chamber shown in figure 5.1 situated on top of an x-y translational stage. The laser beam size was 1.3mm by 1.3mm with a uniform fluence. Firstly, the chamber was pumped down and refilled with bottled (clean) air to reduce any contaminants already present in the chamber. The safety limit of the fused silica windows is higher than the force the vacuum pump could produce. Therefore the chamber was reduced in pressure by 1 bar, and then refilled to an absolute pressure of 1 bar. This process was repeated 4 times. The G-code programme controlling the laser and sample movement exposed the sample for 15 mins at a fluence of $130\text{mJ}/\text{cm}^2$ and a pulse frequency of 50Hz. After irradiation, the laser was turned off, the vacuum pump turned on, and the chamber and pump valves were opened to maintain the pressure at 1 bar. The fume sample and compressed air were drawn past the 2cm fibre for 30 minutes. The fibre was then withdrawn into its housing, removed from the septum, and injected into the GC-MS instrument within ten minutes. Figure 5.2 shows the resultant chromatogram for the XeCl irradiation of a spincoated ITO ink sample on borosilicate dried at 70°C in an oven by INM.

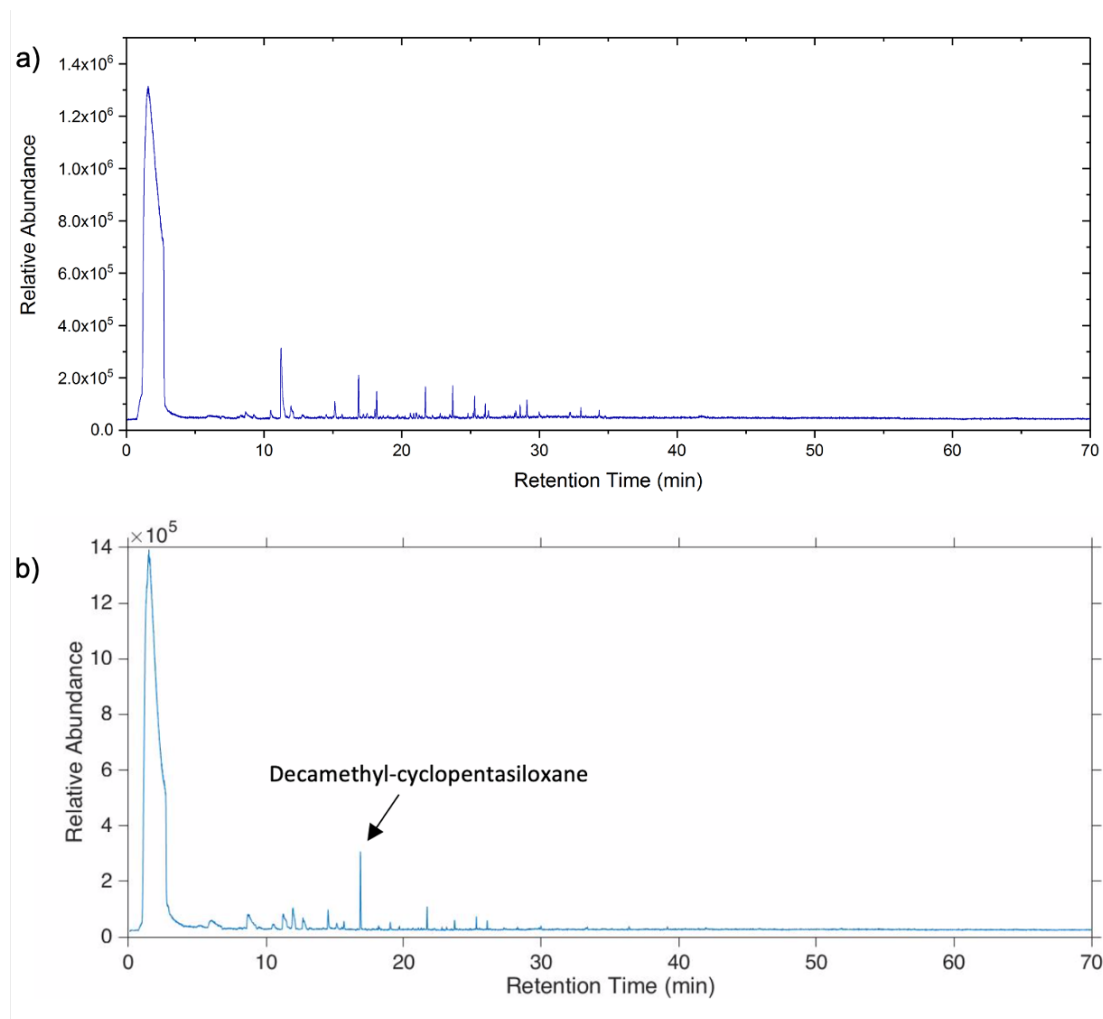


FIGURE 5.2: a) Chromatogram of background with no laser irradiation. b) Chromatogram of ITO nanoparticles, MPTS binder and isopropoxyethanol solvent spin-coated sample irradiated with XeCl for 15 minutes with 2cm SPME fibre extraction for 30 minutes. No fume constituents were identified and the peak at 16.86 min, identified to be decamethyl-cyclopentasiloxane, is column bleed.

No peaks attributed to laser fume generation were detected. The only chemical identification was at 16.86 minutes retention time which was decamethyl-cyclopentasiloxane. This was caused by column bleed.

5.2.2 RF:CO₂ laser irradiation

The chamber cross-flow method shown above in section 5.2.1 was used to irradiate borosilicate glass spin-coated with ITO nanoparticles, MPTS binder and isopropoxyethanol solvent. The SPME fibre was then analysed.

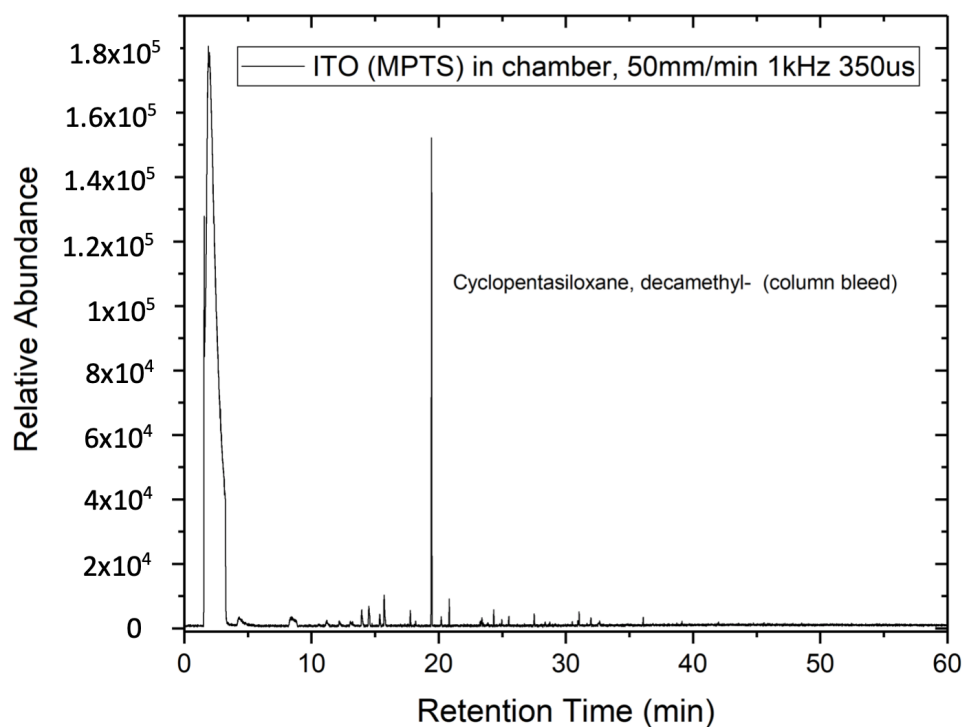


FIGURE 5.3: Chromatogram of ITO nanoparticles, MPTS binder and isopropoxyethanol solvent spin-coated sample irradiated with the $10.6\mu\text{m}$ RF:CO₂ laser within the chamber. The sample was processed with a laser power of 7W, frequency of 1kHz, pulse width of $467\mu\text{s}$, and a duty cycle of 47%. The spot size at the sample was approximately 1mm.

Following RF:CO₂ laser irradiation of dry spin-coated ITO ink films, the chromatogram in figure 5.3 was obtained. Firstly, the chamber was filled, emptied and refilled with compressed air 8 times. The sample was irradiated at 7W, with a spot size of approximately 1mm at the surface, and an overlap of 50%. The

sample velocity was 50mm/min. The sample was irradiated twice to ensure sufficient fume production. The flow was balanced using the inlet and outlet valves of the chamber to give a steady absolute pressure of 1.1bar, as seen on the pressure gauge. The air flow past the fibre had a duration of 30 minutes, after which the SPME fibre was retracted into its housing and injected into the GC-MS port within the next ten minutes for analysis.

Only air and column bleed at 19 minutes retention time were detected. This is probably due to a small proportion of the chamber volume consisting of laser generated fume. The chamber used in this method was significantly larger than the chamber used in section 4.3.

5.3 Direct cross-flow sampling

Direct cross-flow sampling involves the laser generated fume being swept directly past an exposed SPME fibre (figure 5.4), as opposed to the fume being generated and collected in a chamber first. A spincoated ITO MPTS based sample was irradiated with the 193nm ArF laser. An SPME fibre exposed within a T-shaped connector was situated in the flow between a 12V diaphragm pump and the irradiated sample. Copper pipe was used to connect the pump and T-shaped connector and also between the 'T' and fume generated from the sample. Copper was chosen for its inertness. The pump was turned on as irradiation started. Since the sample was manoeuvred on an x-y stage, the sampling end of the copper pipe was situated within 5cm of the beam.

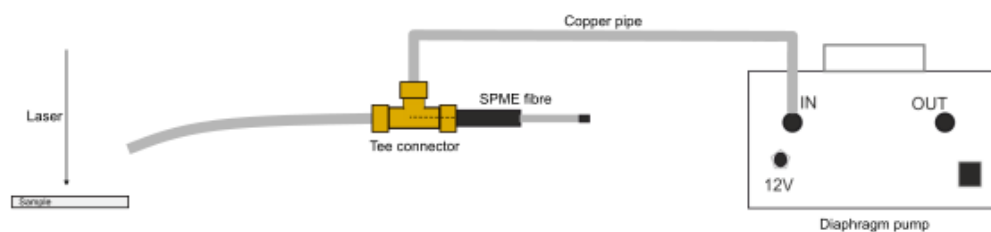


FIGURE 5.4: Schematic diagram of the direct cross-flow technique. Fume from laser irradiation of a sample was drawn past an exposed SPME fibre within a T-shaped connector. The SPME fibre holder was inserted through a septum and the fibre exposed.

Figure 5.5 shows the chromatogram of the resultant fume.

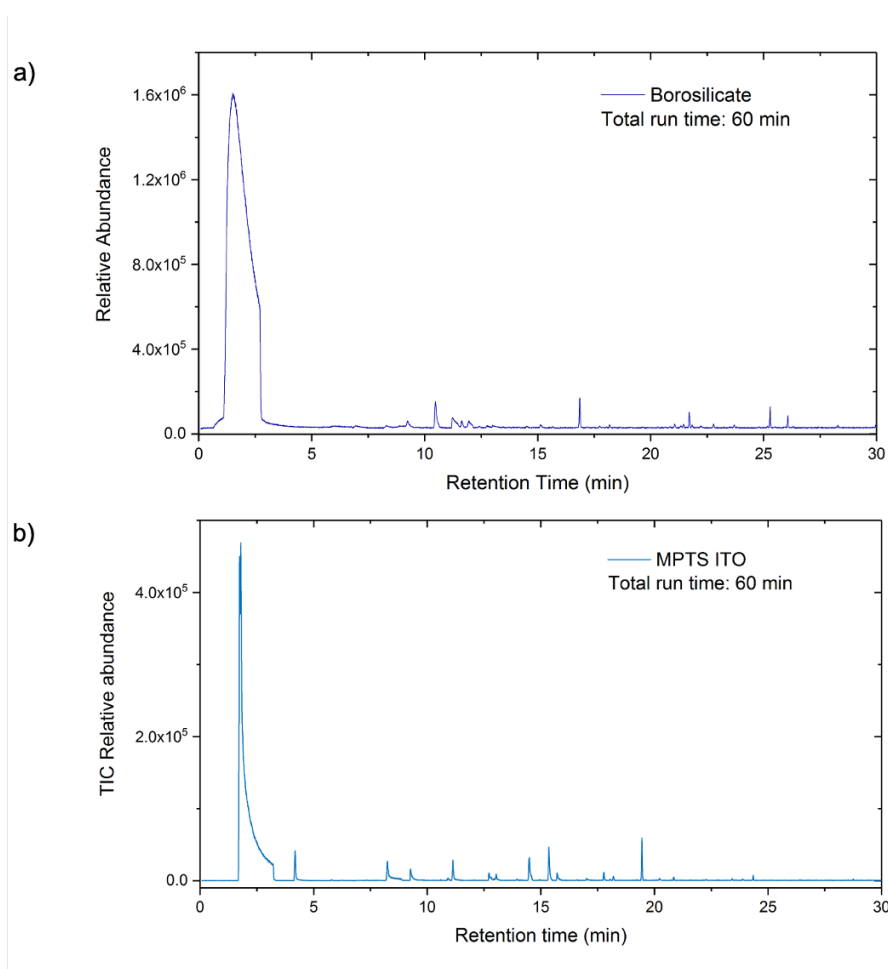


FIGURE 5.5: Comparison of UV irradiation of blank borosilicate glass and spin-coated ITO MPTS sample chromatograms. a) Chromatogram of XeCl (308nm) irradiation of borosilicate glass. b) Chromatogram of a spincoated ITO MPTS on borosilicate glass irradiated with the ArF (193nm) laser at 10Hz for 2 minutes. This was approximately 1200 pulses at a measured fluence of 65 mJ/cm^2 .

Although figure 5.5b shows a few small peaks along with the larger air peak, no conclusive identification was made. This could be due to the laser fume generation not being undertaken in a chamber and therefore being diluted by air. Dilution did not occur to this extent when laser processing was undertaken within a chamber.

5.4 Gas capture

In order to collect laser generated fume in the same proportions as an extraction system, a precise amount of fume and air was collected in a secondary arm. This is termed isokinetic sampling when the flow velocities of the extraction pipe and sampling tube are matched, as explained in chapter 2.

In order to calculate the flow rates for isokinetic extraction as theorised in chapter 2, the diameter of the sampling nozzle was required. Therefore, this was measured using a calibrated optical microscope, (figure 5.6).

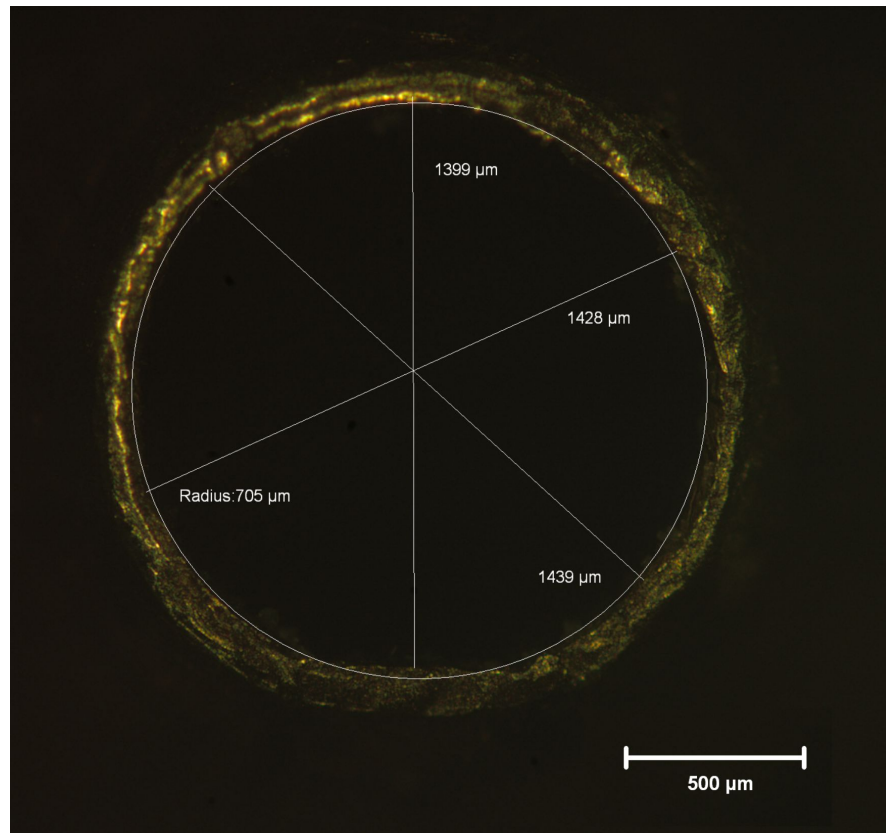


FIGURE 5.6: Cross-section of the sample nozzle orifice imaged using a calibrated optical microscope. The diameter was required to calculate isokinetic flow rates. [16] The image supports the assumption the sample nozzle has a circular cross-section.

Using equation 2.4.1, a volumetric flow rate of 1.6L/min was necessary to match velocities with the 50mm extraction pipe. The extraction volumetric flow rate was 127m³/hr. The velocity in the sample tube therefore needs to be 18m/s in order for the isokinetic condition to occur. This can be measured with a hot-wire anemometer.

One other isokinetic condition was used in order to test the lower limits of the equipment. The fume extractor volumetric flow rate was 79m³/hr, flow meter flow rate 1.0L/min, and the velocity in the sample tube was verified to be 11m/s.

5.4.1 Tedlar bag sampling

The collection method first used was a 1L Tedlar bag as shown in figure 5.7.

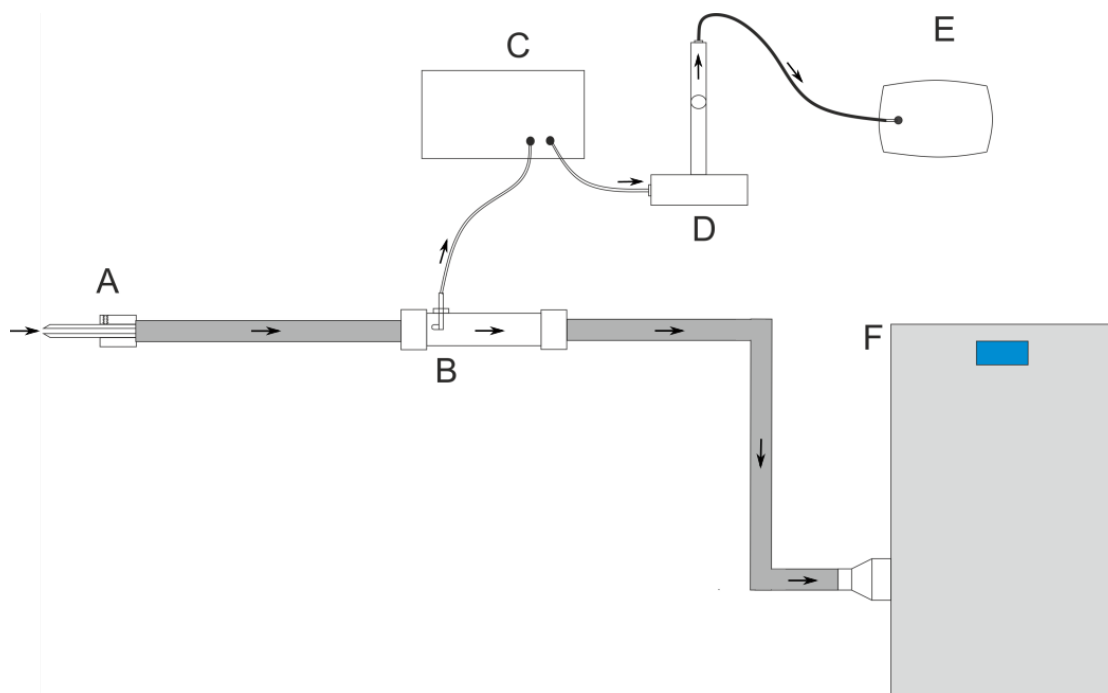


FIGURE 5.7: Complete set up of the isokinetic system. Fume generated by laser irradiation is drawn in through the sampling nozzle [A] by the fume extractor [F] [51] air flow. The diaphragm pump [C] then isokinetically samples a portion of fume and air through the isokinetic sampling tube [B], through the flow meter [D] and into a Tedlar bag [E]. The flow meter controls the air flow of the isokinetic system with a needle valve. The arrows show the direction of air flow. A-sampling nozzle, B-isokinetic sampling tube, C-diaphragm pump, D-flow meter, E-Tedlar bag, F-Purex fume extractor

The isokinetic system was set up with silicone tubing between the isokinetic nozzle, inlet and exit ports of the diaphragm pump, flow meter, and Tedlar bag. The sampling nozzle was then held above the laser irradiation target area at a distance of 10cm. The pump was activated when irradiation started and the resultant fume collected until the Tedlar bag was 2/3 full. Firstly, a sample was taken without the laser in order to give a “blank” reference sample. Chemicals that may have contaminated the gas due to the Tedlar bag were also examined [24].

In order to concentrate the fume an SPME fibre was used as described in section 4.1.1. A silica coated fibre was inserted into the Tedlar sample bag via the septum and then exposed. An adsorption time of 15 minutes was first used due to the literature [25, 52] however this was subsequently changed to 60 minutes adsorption whilst in an oven at 60°C in order to prevent condensation of the fume sample whilst SPME sampling of the analytes.

A sample of air alone was flowed through the system and collected in the Tedlar bag at a flow meter rate of 0.89L/min and Purex fume extractor [51] rate of 79m³/hr. The 2/3 fill time was approximately 45 seconds. Flow velocities were verified with the use of a hot-wire anemometer. A conditioned SPME fibre was then inserted through the valve septum, and the bag with exposed fibre placed in an oven at 60°C for 1 hour. The fibre was then analysed in a GC-MS instrument, as in chapter 4. An example of the resultant control chromatogram is shown in figure 5.8.

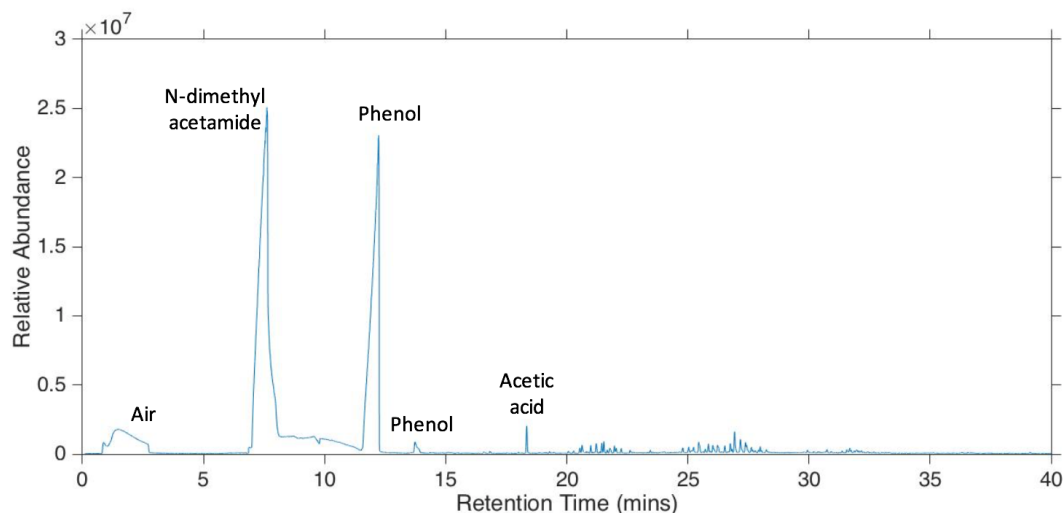


FIGURE 5.8: Chromatogram of a blank air sample. The air was collected through the isokinetic system into a Tedlar bag. An SPME fibre was then inserted through the septum in the bag, heated for 1 hour at 60°C for analyte adsorption, then injected into a GC-MS machine for analysis. The top three substances found in this analysis were N-dimethyl acetamide(RT 6.88-10.66), phenol(RT 12.24,13.53), and acetic acid(RT 18.35). These substances have been labelled.

Three substances were found in this instance and were N-dimethyl acetamide, phenol, and acetic acid. Both dimethyl acetamide and phenol are substances found when analysing new tedlar bags [24]. The production of these analytes may be further encouraged by introducing the Tedlar bag to a temperature of 60°C for 1 hour in order to avoid condensation of the laser generated fume.

The SPME fibre with the adsorbed sample from the Tedlar bag was directly exposed to the GC injector for 5 minutes. The GC injection port is maintained at a high temperature and de-adsorbs all analytes from the fibre, this is the same process as fibre conditioning. The carrier gas, helium, is flowed through the port to the main GC column, moving the sample. The GC injection port was maintained at a temperature of 250°C, as in previous experiments. However in this experiment the ion source in the mass spectrometer had a increased temperature

of 195°C. The results were plotted as a relative abundance versus retention time chromatogram. Lee et al. [21] mentioned that the scanning mode of the mass spectrometer was not sensitive enough (did not show as sharp peaks) with respect to environmental monitoring of VOC's in the workplace, so they used selected ion monitoring (SIM) instead for all their data. They also found that substances with low molecular weight e.g. chloromethane, showed poor results with this technique. The optimisation in section 4.2 showed that it was possible to detect methanol via SPME and GC-MS which has a molar mass of 32.04 g/mol, and therefore it is likely that compounds as light as chloromethane, with a mass of 50.49g/mol, would be possible to detect. Scanning mode was used originally in the project and results showed the peak sharpness observed was adequate.

In order to establish the accuracy of results, 'target' compounds that were previously identified were selected in order to compare their chromatograms, and therefore how they varied with laser regime. This is shown in figure 5.9.

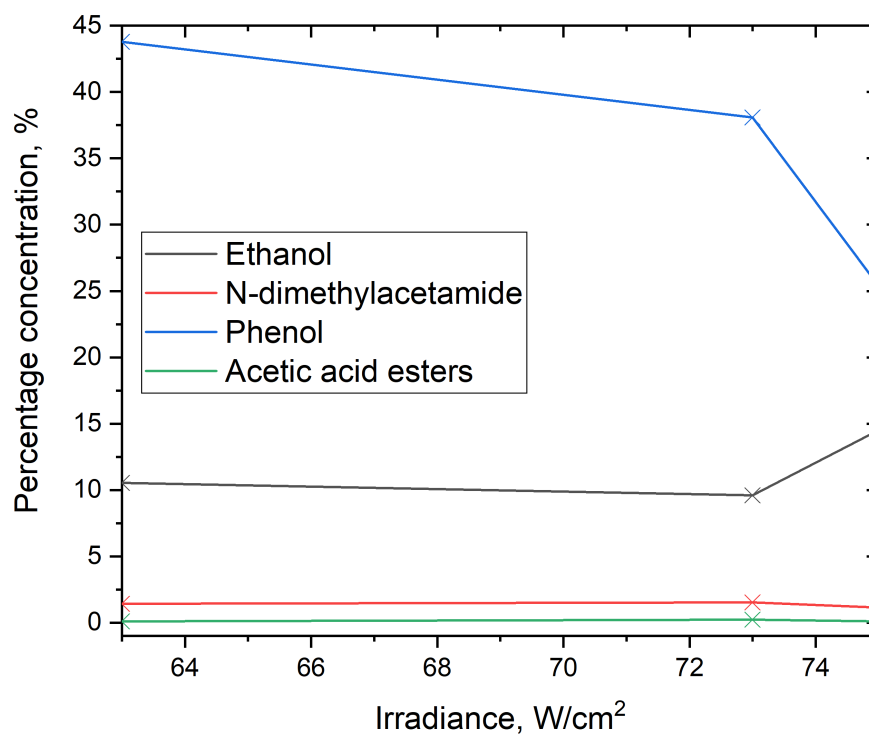


FIGURE 5.9: Percentage concentration of compounds identified in fume samples as a function of irradiance. Percentage concentration is calculated by the GC-MS machine using the integral of the identified chemical peaks. Since this graph does not contain all chemicals identified, the percentages do not total 100%. This was the first study of ITO under different laser regimes with the $10.6\mu\text{m}$ RF:CO₂ laser. This was using the Tedlar bag system which explains the presence of phenol. This explains why the percentage of phenol decreases as the production of other fume becomes more plentiful as the irradiance of the laser increases.

Fig. 5.9 shows the percentage concentration of fume produced for three different $10.6\mu\text{m}$ RF:CO₂ laser regimes, 63, 73 and $75\text{W}/\text{cm}^2$. The amount of fume produced increased with laser irradiance, confirmed by the increased peak size of the target chemicals in the GC-MS chromatograms. It is possible to theorise which substances originated from the Tedlar bag in the fume sample as those for which the percentage concentration decreases as the irradiance of the laser increases. This is due to the increased amount of laser generated fume causing a decrease

in the percentage concentration of constant substances, for example phenol, N-dimethylacetamide and acetic acid.

5.4.2 Glass chamber sampling

Due to the persistent presence of phenol-related features in the chromatograms (as seen in figure 5.8 and 5.9), it was suspected that they may be due to contamination originally from the pipework and Tedlar bag. Therefore, a glass and metal collection system was designed. The system replaced the Tedlar bag with a glass fume collection chamber (figure 5.10) adjacent to the sample nozzle as shown in figure 5.11. Furthermore, the system below ensures the fume sample enters the collection chamber directly and there is no risk of contamination by other components that have been in contact with previous samples. In figure 5.7, the fume was transported through both the diaphragm pump and flow meter before being collected in the Tedlar bag. The glass chamber system is an improvement in the sampling process as well as the materials.

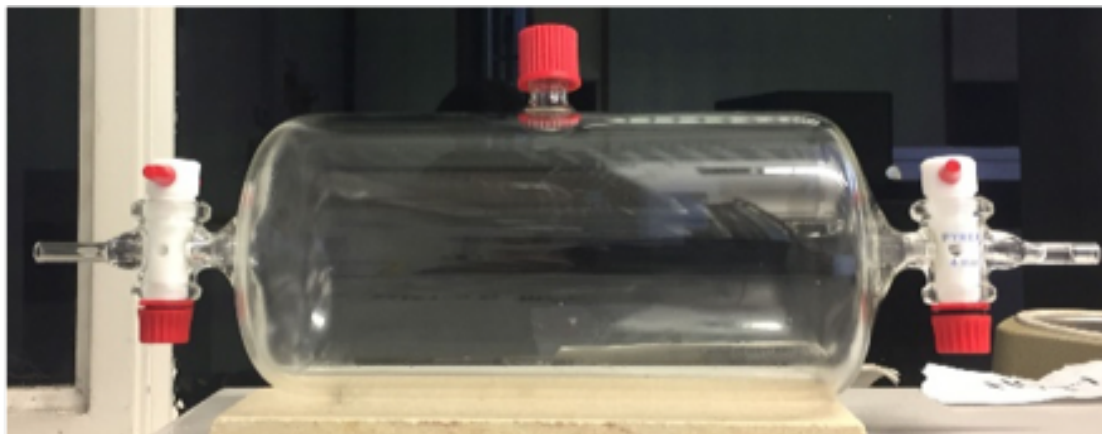


FIGURE 5.10: Glass fume collection chamber of measured volume 0.86L. Poly-tetrafluoroethylene (PTFE) fittings show no thermal degradation below 300°C.

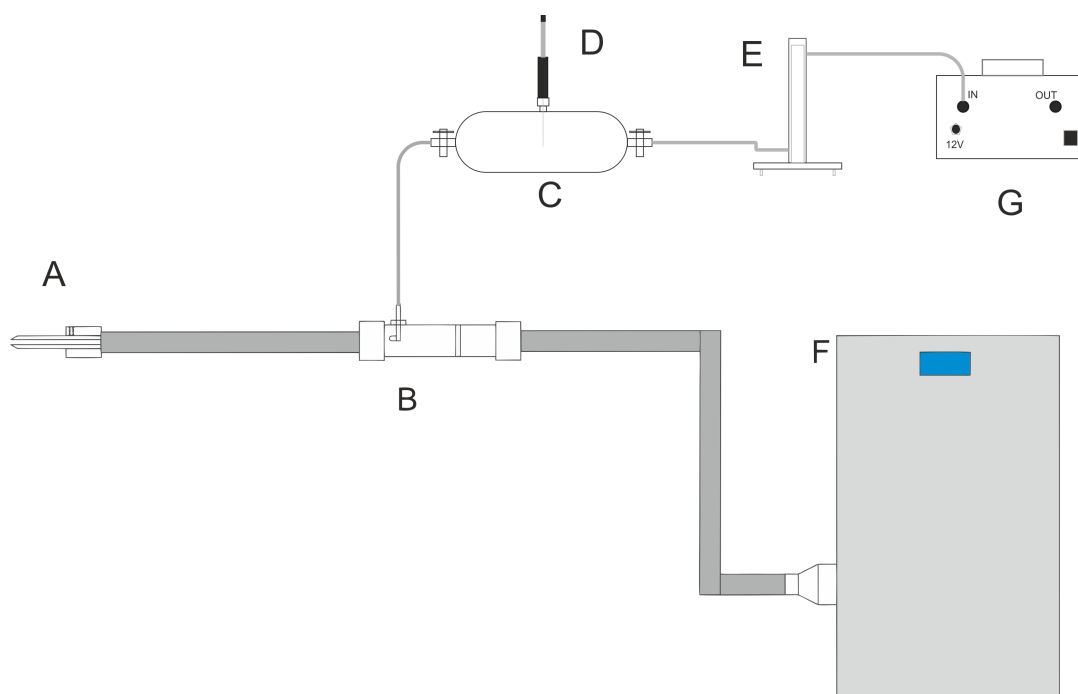


FIGURE 5.11: Isokinetic sampling system used to collect laser fume above the laser interaction site. The fume extractor creates a constant air flow through the system. The diaphragm pump matches this volumetric flow rate and draws a portion of the air and fume into the glass chamber. This chamber is then removed from the system and put in an oven at 60°C for an hour with an inserted SPME fibre. The analytes adsorb onto the fibre which is then inserted into a GC-MS machine and the analytes are identified. A-sampling nozzle, B-isokinetic sampling tube, C-glass chamber, D-SPME fibre, E-flow meter, F-Purex fume extractor, G-diaphragm pump.

In order to test whether this system had now removed contaminants, air was drawn in and the normal sampling process completed. Nothing but the air peak was shown on the chromatogram, as shown in figure 5.12, therefore an improvement was made in removing contaminants.

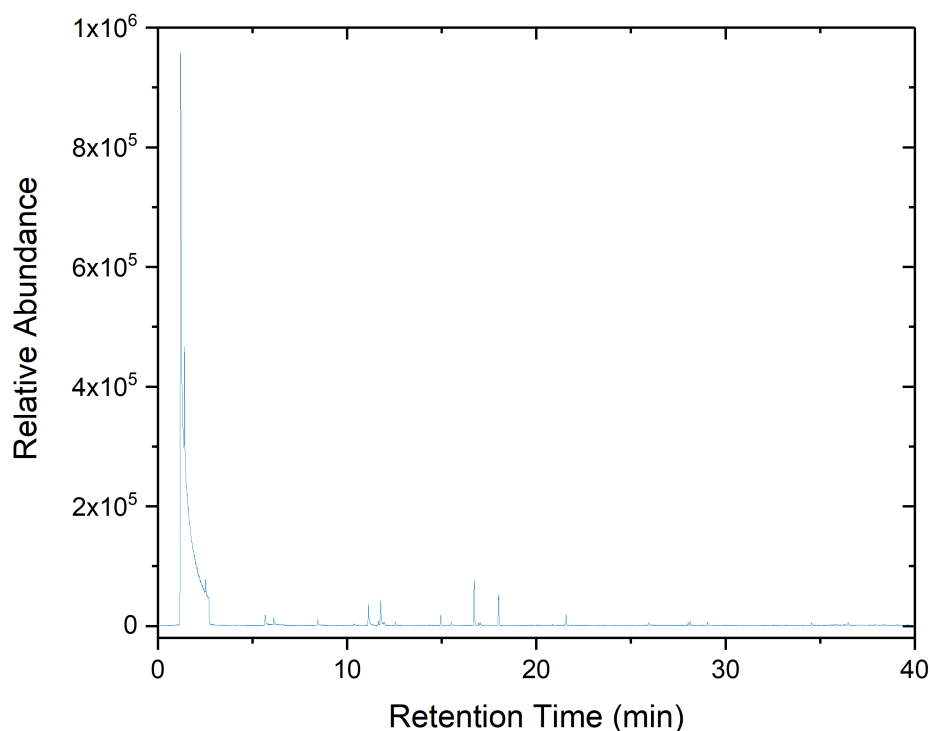


FIGURE 5.12: Chromatogram of laboratory air drawn through the metal-glass system. Adsorption to the fibre occurred for 20 minutes inside the oven at 60°C with the fibre exposed inside the glass chamber. A significant air peak can be seen with a few insignificant peaks at a much lower relative abundance. These either originate from the solvent used to clean the glass chamber (acetone) or column bleed within the GC-MS (siloxanes).

No phenol or dimethylacetamide was found in the analysis proving the glass-metal system was an improvement from the Tedlar bag and compounds that were not associated with laser fume have been removed.

5.4.2.1 XeCl laser irradiation

The 308nm wavelength XeCl excimer laser was used to irradiate two dried spin-coated ITO films on borosilicate glass, with isokinetic fume sampling with the improved glass and metal system.

Firstly, a 50mm by 50mm spin-coated ITO film sample was irradiated in a rectangular spiral starting near the centre of that area by a 1.3mm square beam (at the surface of the sample) at a fluence of 65mJ/cm². The sample velocity was 50mm/min. The flow meter flow rate was set to 1.6L/min and the fume extractor to 127m³/hr. The flow velocity was verified in the sampling tube to be 18m/s. Assuming an incompressible flow through the system and fume generation immediately with laser irradiation, it was calculated that the glass chamber would be filled with one volume of fume and air after 32 seconds. However to be certain fume generation had started the flow was ceased after 90 seconds and the glass chamber taps were closed. The chamber was then removed from the system, an SPME fibre inserted through the septum and exposed, and placed in an oven at 60°C for 1 hour to prevent condensation, in order for the analytes in the fume to be adsorbed. The SPME fibre was then retracted into its housing, removed from the septum, and injected directly into the GC-MS. The resultant chromatogram is shown in figure 5.13.

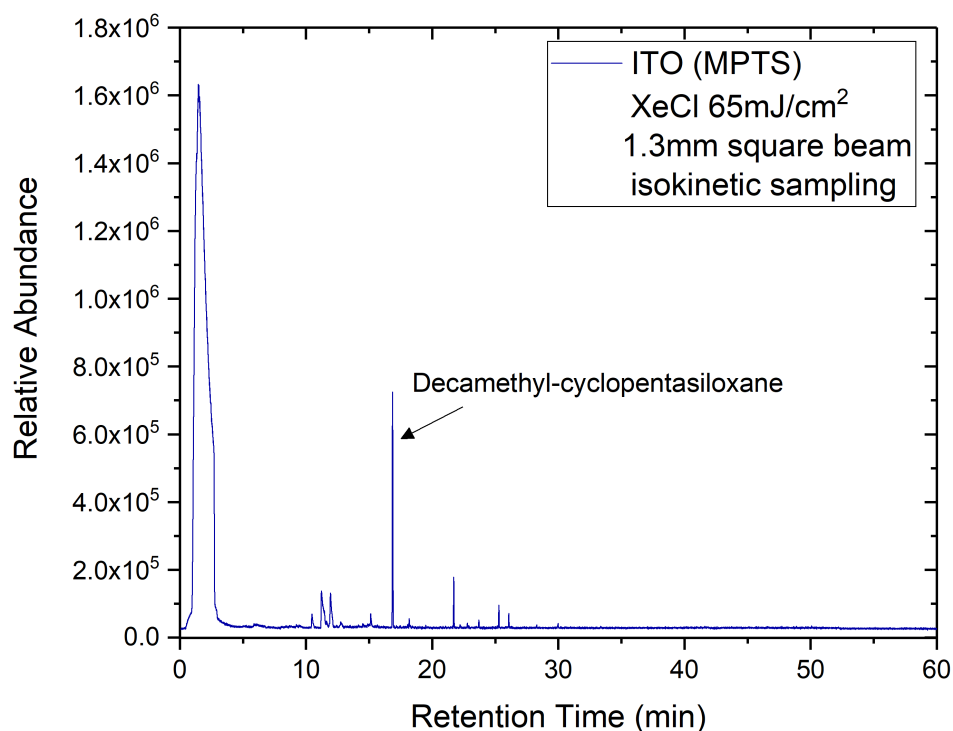


FIGURE 5.13: Chromatogram of XeCl irradiation of a spin-coated dry ITO film sample on borosilicate glass. The sample was irradiated for 90 seconds at 65mJ/cm², with a 1.3mm square beam.

The only significant peak is at 16.86 minutes retention time, decamethylcyclopentasiloxane, which is caused by the stationary phase of the GC column leaking into the mass spectrometer. This is also the case for the peaks at 11.95 and 21.76 minutes which are octamethyl-cyclotetrasiloxane and dodecamethyl-cyclohexasiloxane respectively. No peak attributed to laser-generated fume was detected.

Secondly, a 50mm by 50mm spin-coated ITO film sample was irradiated at approximately twice the previous fluence. Irradiation was undertaken in a rectangular spiral starting near the centre of that area by a 1.6mm by 1.6mm square beam (at the surface of the sample) at a fluence of 120mJ/cm². As above, the flow meter

flow rate was set to 1.6L/min and the fume extractor to 127m³/hr. The flow velocity was verified in the sampling tube to be 28m/s. The sample was irradiated for 90s before the glass chamber taps were closed and it was removed from the system. The SPME fibre was inserted into the chamber via the septum, exposed, and placed in an oven for 1 hour at 60°C. Once removed, the SPME fibre was injected into the GC inlet port for analysis. The resultant chromatogram is shown in figure 5.14.

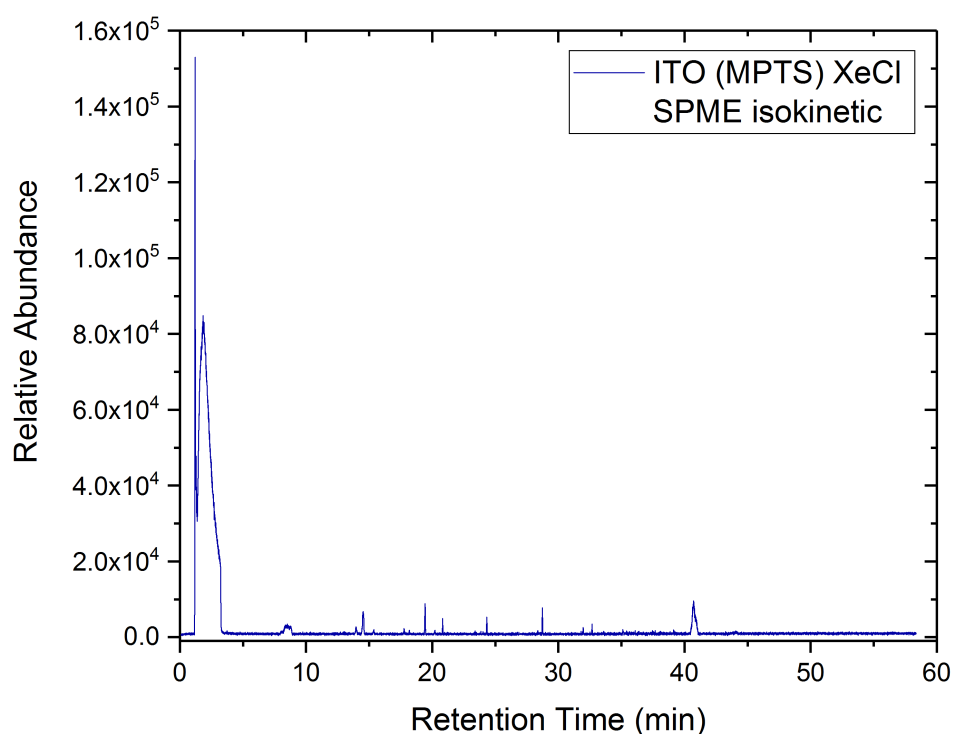


FIGURE 5.14: Chromatogram of XeCl irradiation of a spin-coated dry ITO film sample on borosilicate glass. The sample was irradiated for 90 seconds at 120mJ/cm², with a 1.6mm square (at the surface) beam.

The only significant peak was at 1.206 minutes retention time which was methane. This was not thought to be generated by laser fume. Doubling the UV fluence

applied to the ITO film samples did not appear to generate or increase the level of detected fume.

5.4.2.2 RF:CO₂ laser irradiation

Another 50mm by 50mm MPTS based ITO film was irradiated with the 10.6 μ m continuous wave RF:CO₂ laser and the fume sampled by the glass chamber isokinetic system. The laser output was modulated at a frequency of 998Hz and the pulse width was set to 463 μ s. This was a duty cycle of 47%. The laser power was 11W and the unfocussed beam was used, which was 3.8mm in diameter. This equates to an irradiance of 97W/cm². The flow rate was set to the same conditions as in section 5.4.2.1, and irradiation undergone for the same duration. The resultant chromatogram is shown in figure 5.15.

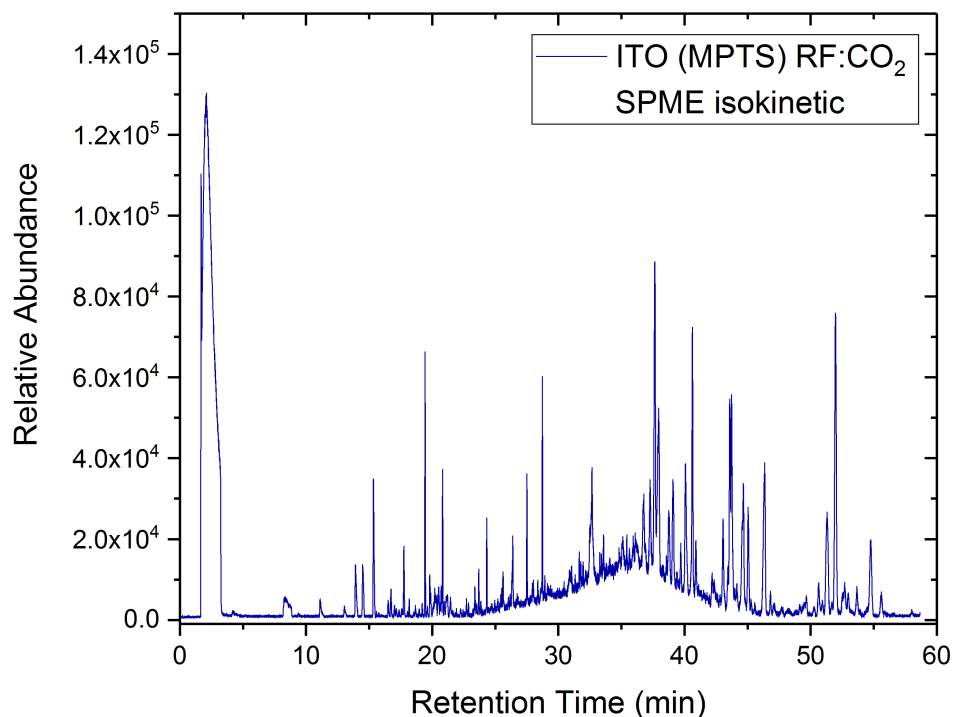


FIGURE 5.15: Chromatogram of a spin-coated dry ITO ink film sample on borosilicate glass. Irradiated with the RF:CO₂ for 90s at a frequency of 998Hz, and pulse width of $463\mu\text{s}$. The beam was unfocused and had a diameter of 3.8mm at the surface of the sample.

No conclusive matches were found except decamethyl-cyclopentasiloxane and di-n-octyl phthalate. The former is column bleed and the latter was not judged to be collected by the SPME fibre. Di-n-octyl phthalate has a molecular weight of 390.56g/mol which is far outside the mass range of the SPME fibre used. It was determined that this compound was from contamination in the GC-MS, and not from laser irradiation of the ITO film. The distorted baseline is due to a hydrocarbon oil coming into contact with the SPME fibre. Since no rotary vane pumps were used in the system and the fibre was conditioned before the experiment, the hydrocarbon oil must have originated from the GC-MS inlet from another use.

Long chain hydrocarbons cannot be resolved into peaks as they are broad. The hydrocarbon oil can be removed from the fibre by conditioning in the GC inlet port.

5.4.3 Discussion

Firstly, a sample of laboratory air was collected through the system shown in figure 5.7 into a Tedlar bag. When the adsorbents on the SPME fibre were analysed by the GC-MS, Tedlar bag sampling was shown to detect elements of the Tedlar bag itself, as shown in section 5.4.1. Then borosilicate glass samples spin-coated with ITO nanoparticles, MPTS binder, and isopropoxyethanol solvent were irradiated at different IR irradiances and the previous unwanted analytes were again detected. The presence of dimethyl acetamide and phenol were eradicated with the use of a glass-metal system. This system still did not detect laser-generated fume however. This could be due to little fume generation, or the system may not be sensitive enough to detect the fume produced.

With the glass-metal system the XeCl and RF:CO₂ lasers were used to irradiate borosilicate glass samples spin-coated with ITO nanoparticles, MPTS binder, and isopropoxyethanol solvent. The XeCl showed no conclusive laser generated fume peaks but did show column bleed. To try and mitigate column bleed, the GC-MS oven was left at 300°C overnight to clean the column which did not succeed in mitigating future column bleed.

RF:CO₂ laser irradiation did not produce conclusive fume peaks. It was not expected that any conclusive fume peaks would be observed when irradiating the glass samples with an irradiance of 97W/cm² since in section 5.2.2, an irradiance of 891W/cm² was used and no peak attributed to laser generated fume was found.

The dilution factor between the chamber method in chapter 4 and the isokinetic system utilised in section 5.4.2 is important to note. During isokinetic sampling, the material is irradiated for 90 seconds. During that time, approximately 5000 chamber volumes passed through the sampling tube. Also within the sampling tube, the isokinetic nozzle only accounts for a small proportion of the area. There is an additional dilution factor of 69:1. Therefore, the likelihood of observing significant peaks similar to the chamber sampling chromatograms is low. The advantage of using this set up (figure 5.11) is that it can be incorporated within an industrial flow line so sampling can occur at any time.

The Tedlar bag reduced the dilution factor of the fume, but the phenol could not be ignored since it made up up to 45% of samples as shown in figure 5.9.

In summary, the sampling process was improved by the modification of the collection method. No fume peaks were detected via the isokinetic sampling method. Since the gas sampled with this technique was similar to an extraction flow during industrial laser material processing, it is a positive result that laser generated fume was not detected.

5.5 Particulate sampling from a gas flow

To sample particulates from a gas flow, adhesive slides called witness plates were used. A spin-coated ITO ink borosilicate sample was irradiated within a chamber.

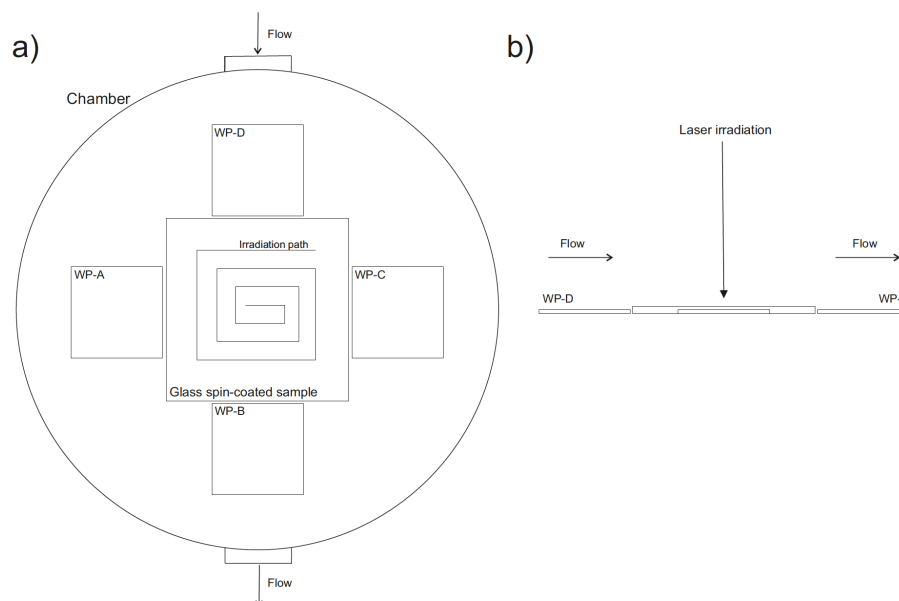


FIGURE 5.16: Schematic of the witness plates surrounding the spin-coated borosilicate glass sample with the chamber. a) shows the aerial view parallel with irradiation of the sample. Shown are the four 25mm by 25mm witness plates made from adhesive coated microscope slides. b) illustrates a side profile of the sample and witness plates in the chamber. The flow created by opening a valve between an air cylinder and vacuum pump moves from WP-D to WP-B.

Particulate ejecta from the laser interaction site may result from the ITO nanoparticles or ablation of the substrate. Glass slides coated in adhesive, acting as “witness plates”, can be used to capture and view particulates. When witness plates were used in the static sampling method, no laser-induced particulates were observed. Due to the higher fluence involved with irradiation by the XeCl excimer laser, witness plates 25mm by 25mm in size, were situated on each side of the spincoated borosilicate glass sample within the chamber. The witness plates were expected to capture any laser generated particulates that succumbed to gravity

within the chamber. They would therefore be secured in place when a flow was created through the chamber for the SPME analysis.

Following exposure, these adhesive slides were subjected to inspection by electron microscopy and any particles observed analysed for composition by the integrated energy-dispersive X-ray analysis (EDXA) facility. Figure 5.17 and 5.18 show the presence of approximately 40nm diameter particulates which were identified by EDXA as ITO.

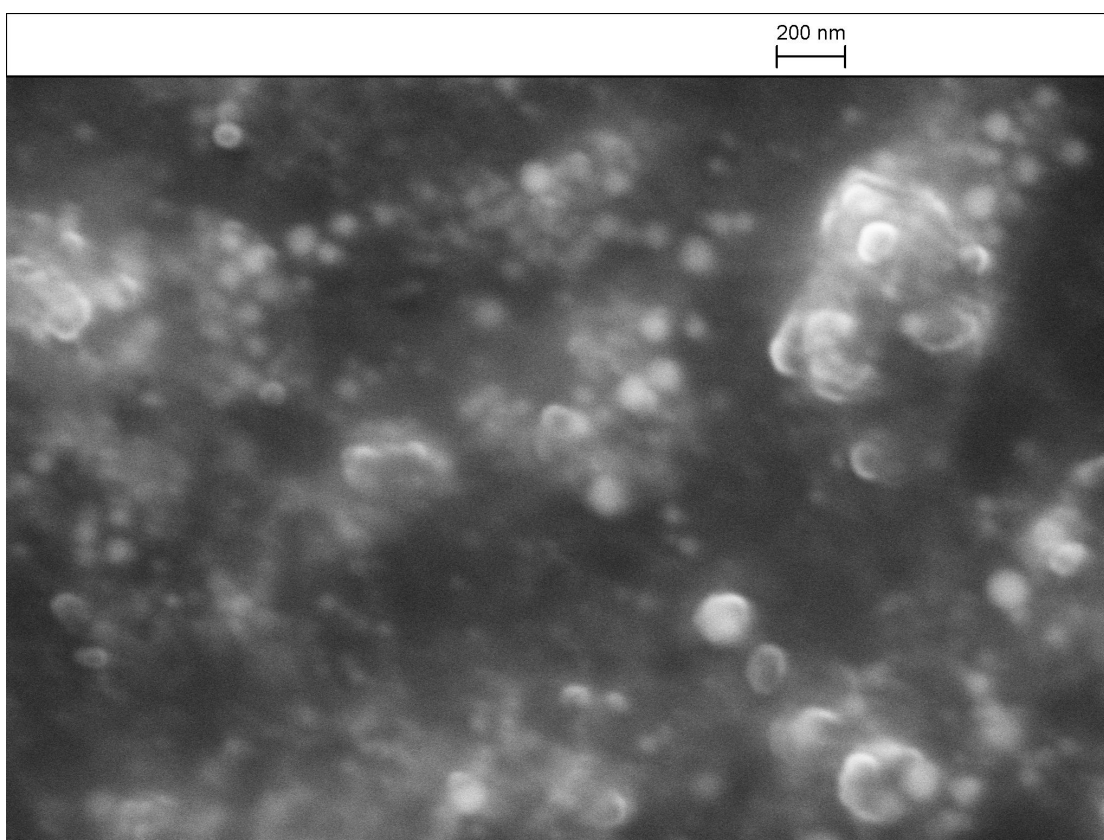


FIGURE 5.17: SEM image of indium and tin particulates approximately 40nm in size.

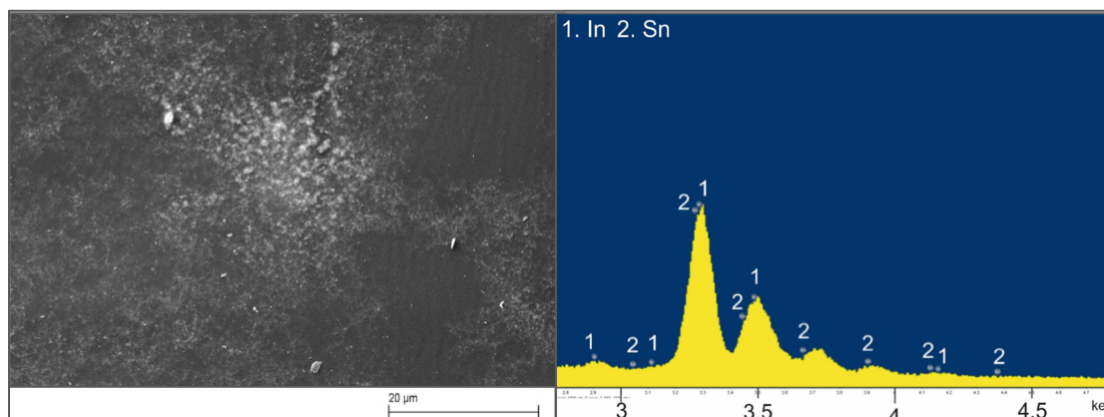


FIGURE 5.18: SEM image of 40nm ITO particles identified by EDXA. These particulates were ablated via a 308nm UV XeCl laser from a spin-coated ITO ink borosilicate glass sample at a fluence of 130mJcm^{-2} .

Figure 5.16 shows the flow moving through the chamber from the valve by WP-D, to the valve by WP-B. The particulates in figure 5.17 were detected from WP-B. This witness plate collected the most particulates. This is due to WP-B being between laser-induced particulate generation and the exit port of the chamber. The origin of the nanoparticles may also be ITO particles that succumbed to gravity during irradiation. Particulates of 40nm in diameter were expected to be released during irradiation due to ITO nanoparticles of that size being used in the manufacture of the ink [32]. It has been suggested that a reaction with oxygen can lead to clusters as seen in figure 5.17 [53].

5.6 Discussion

This chapter involved the sampling of laser fume from a flow, after and during irradiation, collection of gas containing fume for analysis later, and particulate sampling from a flow.

The system shown in figure 5.1 has the advantage of increasing the sample concentration similar to the Tedlar bag in the early isokinetic system. The closed chamber method had a considerably shorter duration than the isokinetic method due to the SPME fibre being immediately ready for GC-MS analysis after the carrier gas containing the fume was flowed past. This method also had the advantage of different atmospheres and pressures for laser processing. In the parallel studies of improving the conductivity of these materials, it was found working in a controlled atmosphere was advantageous. In this way, SPME sampling and conductivity improvement can occur simultaneously. Vacuum pressures cannot be achieved when using the RF:CO₂ laser due to the inclusion of salt windows in the chamber. The pressure differential calculated for the dimensions of the NaCl windows was $\Delta P=0.66$ bar, moreover the structural integrity of the windows was uncertain 0.33 bar above or below atmospheric pressure.

The only presence of particulates detected was under 130 mJcm⁻² XeCl UV irradiation. These were collected on adhesive witness plates and examined under SEM, (figure 5.17). It is apparent that laser irradiation under UV makes significant changes to the structure of the films when comparing with figure 3.1, the unirradiated film. Figure 5.18 proves the particulates are ITO via EDXA.

5.7 Conclusion

The data in this chapter shows that all gaseous results were inconclusive. Moreover, the laser regimes and sampling methods used did not provide measurable

outcomes or compound identification of laser generated fume via GC-MS. It's possible that gases were produced but they were masked by contaminants from the Tedlar bag. Therefore the glass chamber method is most appropriate.

Particles that are 40nm in diameter are too small to be captured by any class of HEPA filter, the smallest filter having a resolution of $0.3\mu\text{m}$ and an efficiency of 99.97% [54]. The presence of ITO particles shows damage of the ITO film due to ablation. Since ablation can reduce the conductivity of the films, this result shows that this laser regime is not suitable for the process under consideration.

In summary, all laser regimes used below the damage threshold of the materials irradiated did not produce enough laser-generated fume to be detectable by isokinetic SPME sampling. However, for fluences higher than the damage threshold of the ITO films, particulates were observed.

Future work should consist of completing the isokinetic sampling process with the SPME fibre exposed within the glass chamber, whilst the laser generated fume and air is drawn past, before the taps are closed. This would combine the current process with the cross-flow method from section 5.3, which should increase adsorption onto the fibre.

Hazard Assessment

6.1 Introduction

This chapter will provide an overview of the chemicals identified from the fume analysis process, the hazards they present, and their exposure limits. Also, mitigation strategies will be suggested for any fume produced in the laser processing of ITO thin films. Analysis of the hazards presented by the material safety data was undertaken and the chemicals with the highest toxicity specified. To specify the type of mitigations that should be in place, such as the filters required, it is necessary to know the composition of the fume. This was the aim of chapters 4 and 5. Below is a summary of all chemicals used or identified in this research. Some abbreviations used within this chapter include: STEL - short term exposure limit, TWA - time weighted average, LD50 - lethal dose 50%, LD0 - maximum tolerable concentration, LC50 - median lethal concentration, LDLO - lowest lethal dose. For full definitions see the following references [55, 56].

6.2 Review of MSDS data

This section will give a brief overview of the material safety data for the chemicals identified via GC-MS in the laser produced fume. The mitigation techniques outlined are only suitable for contact with large amounts of the chemicals. Since the

chemicals below were identified in very small amounts, such stringent mitigations may not be necessary for laboratory scale experiments, but are worth considering for factory-scale manufacture.

6.2.1 ITO nanoparticles

ITO occurs as a yellow powder containing nanoparticles approximately 25nm in diameter. Mitigations for exposure to ITO nanoparticles include wearing a National Institute for Occupational Safety and Health/Mine Safety and Health Administration (NIOSH/MSHA) approved respirator, safety glasses, and impermeable gloves and personal protective equipment (PPE). Avoid forming dust and use local exhaust ventilation with a HEPA filter [57]. The information contained in reference [57] is summarised in table 6.1.

TABLE 6.1: Material hazard information for ITO[36, 57].

Material hazards	
CAS number	50926-11-9
Classification	Specific target organ toxicity - repeated exposure, category 1
Hazard statements	H372 Causes damage to lungs through prolonged or repeated exposure
Exposure limits	Diindium trioxide - TWA 0.1mg/m ³ , STEL 0.3mg/m ³ Tin (IV) oxide - TWA 2mg/m ³ , STEL 4mg/m ³

6.2.2 Isopropoxyethanol

Isopropoxyethanol was used to dilute the mixture of nanoparticles and MPTS binder in the ink. It was also identified in the fume analysis in section 4.4. Mitigation techniques to avoid exposure include wearing safety glasses and face mask, a flame retardant laboratory coat, and gloves. Do not dispose of waste down the drain [36]. The information contained in reference [36] is summarised in table 6.2.

TABLE 6.2: Material hazard information for isopropoxyethanol.

Material hazards	
CAS number	109-59-1
Classification	Flammable liquids (Category 3) Acute toxicity, Inhalation (Category 4) Acute toxicity, Dermal (Category 4) Skin irritation (Category 2) Eye irritation (Category 2)
Hazard statements	H226 Flammable liquid and vapour. H312 + H332 Harmful in contact with skin or if inhaled. H315 Causes skin irritation. H319 Causes serious eye irritation.
Acute toxicity	LD50 Oral - Rat - 5117 mg/kg LC0 Inhalation - Rat - male - 4 h - > 3500 ppm LD50 Dermal - Rabbit - male - 1440 mg/kg

6.2.3 MPTS

The MPTS or 3-Methacryloxypropyltrimethoxysilane, sometimes known as 3-(Trimethoxysilyl)propyl methacrylate, was used as a binder and along with the ITO nanoparticles and IPE formed the ink. A thermal fragment of MPTS was found during the static sampling of MPTS spin coated on glass in figure 4.8. Mitigations against exposure include the relevant PPE such as gloves, laboratory coat

and safety glasses. If spillage occurs absorb with a liquid-binding material such as sand or sawdust. Use a local exhaust system or work within a fume cupboard wherever possible [35, 58]. The information contained in references [35, 58] is summarised in table 6.3.

TABLE 6.3: Material hazard information for MPTS [35, 58].

Material hazards	
CAS number	2530-85-0
Classification	STOT SE (Category 3) Skin irritation (Category 2) Eye irritation (Category 2)
Hazard statements	H315 Causes skin irritation. H335 May cause respiratory irritation. H319 Causes serious eye irritation.
Acute toxicity	LD50 Oral - Rat - male and female - > 2000 mg/kg LC50 Inhalation - Rat - male and female - 4 h - > 2.28 mg/l LD50 Dermal - Rat - male and female - > 2000 mg/kg

6.2.4 Butyl methacrylate

Butyl methacrylate was identified via static chamber sampling of spincoated MPTS (4.8) in section 4.4. To avoid exposure to the chemical safety glasses, nitrile gloves, and flameproof laboratory coat. Use local exhaust ventilation (LEV) and work in a fume cupboard where possible [59]. The information contained in references [48, 59] is summarised in table 6.4.

TABLE 6.4: Material hazard information for butyl methacrylate [48, 59]

Material hazards	
CAS number	97-88-1
Classification	Flammable liquids (Category 3) Skin irritation (Category 2) Eye irritation (Category 2) Skin sensitisation (Category 1) Specific target organ toxicity - single exposure (Category 3)
Hazard statements	H226 Flammable liquid and vapour. H315 Causes skin irritation. H317 May cause an allergic skin reaction. H319 Causes serious eye irritation. H335 May cause respiratory irritation.
Acute toxicity	TWA 50ppm STEL 75ppm LD50 Oral - Rat - 16000 mg/kg LC50 Inhalation - Rat - 4 h - 4910 ppm LD50 Dermal - Rabbit - 10125 mg/kg

6.2.5 N-dimethyl acetamide

N-dimethyl acetamide was identified when dynamic sampling with the Tedlar bag system. The chemical was also identified when an ITO thin film was irradiated

with an RF:CO₂ laser at fluences between 63W/cm² and 75W/cm², also sampled with the Tedlar bag system. To avoid exposure a face shield and safety glasses are advised, as well as gloves and a complete suit in case of spillage [60]. The information contained in reference [60] is summarised in table 6.5.

TABLE 6.5: Material hazard information for n-dimethyl acetamide [60].

Material hazards	
CAS number	127-19-5
Classification	Acute toxicity, Inhalation (Category 4)
	Acute toxicity, Dermal (Category 4)
	Eye irritation (Category 2)
	Reproductive toxicity (Category 1B)
Hazard statements	H312, H332 Harmful in contact with skin or if inhaled.
	H319 Causes serious eye irritation.
	H360D May damage the unborn child.
Acute toxicity	TWA 10 ppm, 36 mg/m ³
	STEL 20 ppm, 72 mg/m ³
	LD50 Oral - Rat - 5680 mg/kg
	LC50 Inhalation - Rat - 1 h - 2475 ppm
	LD50 Dermal - Rabbit - 2240 mg/kg

6.2.6 Octamethylcyclotetrasiloxane

Octamethylcyclotetrasiloxane was identified when an ITO thin film was irradiated at 65mJ/cm² with a XeCl excimer laser. Mitigations against exposure include safety glasses, gloves, flame retardant laboratory coat, and a LEV system. Gloves

must be removed without contact with outer surface [61]. The information contained in reference [61] is summarised in table 6.6.

TABLE 6.6: Material hazard information for octamethylcyclotetrasiloxane [61].

Material hazards	
CAS number	556-67-2
Classification	Flammable liquids (Category 3) Reproductive toxicity (Category 2) Chronic aquatic toxicity (Category 4)
Hazard statements	H226 Flammable liquid and vapour. H361 Suspected of damaging fertility or the unborn child. H413 May cause long lasting harmful effects to aquatic life.
Acute toxicity	LD50 Oral - Rat - > 2000 mg/kg LD50 Oral - Rat - male - > 4800 mg/kg LC50 Inhalation - Rat - male and female - 4 h - 36 mg/l LD50 Dermal - Rat - male and female - > 2400 mg/kg

6.2.7 Phenol

Phenol was a large contributor to the sampled fume when using the Tedar bag sampling system. During some experiments the fume contained up to 45% phenol (figure 5.9). Mitigations against exposure must include, butyl rubber gloves for full contact, safety glasses and face shield, and a complete protective suit [62]. The information contained in reference [62] is summarised in table 6.7.

TABLE 6.7: Material hazard information for phenol [62].

Material hazards	
CAS number	108-95-2
Classification	Acute toxicity, Oral (Category 3)
	Acute toxicity, Inhalation (Category 3)
	Acute toxicity, Dermal (Category 3)
	Skin corrosion (Category 1B)
	Serious eye damage (Category 1)
	Germ cell mutagenicity (Category 2)
	Specific target organ toxicity - repeated exposure (Category 2)
	Chronic aquatic toxicity (Category 2)
	Hazard statements
H314 Causes severe skin burns and eye damage.	
H341 Suspected of causing genetic defects.	
H373 May cause damage to organs through prolonged or repeated exposure.	
H411 Toxic to aquatic life with long lasting effects.	
Acute toxicity	TWA 2 ppm, 7.8 mg/m ³
	STEL 4 ppm, 16 mg/m ³
	LD50 Oral - Rat - 317.0 mg/kg
	LC50 Inhalation - Rat - 8 h - 900 mg/m ³
	LD50 Dermal - Rabbit - 630.0 mg/kg

6.3 Analysis of the hazards

The most toxic of chemical found from analysis of the above MSDS data was the ITO nanoparticles. ITO is the most dangerous as the STEL values for diindium

trioxide and tin (IV) oxide were $0.3\text{mg}/\text{m}^3$ and $4\text{mg}/\text{m}^3$ respectively. The TWA values were $0.1\text{mg}/\text{m}^3$ and $2\text{mg}/\text{m}^3$ respectively. These were the lowest safety limits for all fume contents identified by GC-MS. The nanoparticles however, are not expected to be a component of the fume. This is because removal of the ITO signifies damage to the irradiated tracks on the thin films. This means that the conductivity would be reduced and a less-than-optimum material produced.

The above values show that a very large amount of irradiation would be need to produce the amount of fume that constitutes a lethal dose. It is known from the thermal degradation data produced in chapter 3 that the constituents of the ink do not remain the same during irradiation (figure 3.7). Also what is left will be a fraction of the content and is therefore difficult to estimate due to lack of quantitative results. But imagine irradiating a track $20\mu\text{m}$ wide and 400nm deep at a feed rate of $1\text{m}/\text{s}$. If you removed 100% of the material, 40% of which is ITO nanoparticles, inside a laboratory that was 75m^3 , it would take 1.6 hours to accumulate to the STEL value of $0.3\text{mg}/\text{m}^3$ and 32.6 minutes to reach the TWA value of $0.1\text{mg}/\text{m}^3$.

Using the above estimates, for ITO, a flow rate of at least $150\text{m}^3/\text{hr}$ is required to not broach the TWA safety limit during irradiation which is easily achievable by industrial LEV units.

6.4 Conclusion

In this chapter, the hazards for each chemical identified via GC-MS were outlined and the mitigation techniques described. All of the chemicals produced need PPE and local exhaust ventilation (LEV) to reduce the risk of exposure. In practice, it is usual for industrial scale processes to utilise a LEV system to collect any fume. To specify the type of LEV and filters that it must contain, it is necessary to know the composition of the fume. The aim here is to guide this process. In addition, it is a legal requirement that the LEV are regularly inspected for their effectiveness and so it is important to know the nature of the gases and particulates in the environment. Since no quantitative comparison can be made between fume produced in the laboratory and fume produced at factory-scale, local fume should be sampled and analysed in order to more accurately ascertain the hazards to workers.

Furthermore, it can be assumed that it is mainly organics in the fume. Nanoparticles are not expected in the fume since that would mean removal from the irradiated tracks and therefore lower conductivity in the material. Organics will be dealt with by the activated charcoal aspect of an LEV filter. It is recommended to use a LEV unit that can produce flow rates exceeding $150\text{m}^3/\text{hr}$, and that contains a three stage filter system including pre-filter, HEPA filter and activated charcoal. The exhaust of the LEV should be directed outside to further dilute the fume. It is also recommended that personal monitoring is employed to check that the LEV system is successful and that no nanoparticles are present in the fume. This is especially important since respirators do not protect against nanoparticles.

Conclusion

The purpose of this research was to improve knowledge of laser processing by-products so as to inform users and allow them to mitigate any hazards. Chapter 2 showed that other workers have observed particulate clusters, vapour and gas-phase by-products from laser-material interactions. It was shown that the use of UV lasers led to photo-degradation products via direct bond scission and the production of particulate matter. On the other hand, use of IR lasers caused thermal decomposition of the irradiated material, leading to similar by-products as observed by burning. This process lead to vapour and gas-phase chemicals being produced. The by-products observed from these laser-material interactions showed there is a need to sample gas and particulate phase products to learn their composition. Techniques to sample gases were described and processes to capture low concentrations of gases suggested. The SPME fibre approach was used as this was expected to be the most appropriate method as it is inexpensive and mobile, and the isokinetic condition was discussed in order to facilitate a quantitative assessment of the fume. Although particulates can be trapped by HEPA filters their size and distribution can be difficult to visualize due to the fibrous nature of the filter medium, therefore witness plates were suggested as a capture method for EDXA analysis.

Chapter 3 described the materials used in this research such as the components of the ink (nanoparticles, IPE, MPTS), the substrate and the coating technique

used to manufacture the thin films for laser irradiation. It was determined from TGA data that during irradiation, if the laser heats the film to temperatures above 350°C, decomposition fragments of MPTS would be expected in the fume. It was concluded that although the temperature of the material when irradiated was not known, if the laser regime was below the damage threshold of the glass, gas-phase products were still expected in the fume.

Laser fume generated within closed cells and experiments with no extraction were then sampled and analysed in chapter 4. Firstly, the GC-MS method was optimised to increase the resolution in the low mass region. This was visualized by the separation of methanol peaks on the resultant chromatograms from SPME sampling of methanol fume. The peak separation was increased from 0.065 minutes to 0.105 minutes. Some of the thermal degradation products of the ITO films were successfully identified (figure 4.8) within the closed chamber due to the system increasing the concentration of the fume. The static sampling system however was not analogous to the large-scale irradiation of thin films and therefore a dynamic sampling system where fume is collected and analysed from an extraction flow was developed.

A dynamic sampling system was designed that allowed fulfilment of the isokinetic condition between a fume extraction flow and the flow of a secondary arm that included a diaphragm pump and flow meter. The fume was sampled via this secondary arm and collected in a Tedlar bag, into which an SPME fibre was introduced. The Tedlar bag and fibre were then placed in an oven for 1 hour at 60°C in order to mitigate any condensation of the fume and collect the analytes

via SPME. When the SPME fibre was analysed by GC-MS, it was found that up to 45% of the fume consisted of phenol. It was suspected the phenol originated from the polyvinyl fluoride Tedlar bag, therefore a new system was designed that eliminated all polymeric materials. This system still upheld an isokinetic condition with an extraction flow however it now included a glass chamber and metal piping, as well as diaphragm pump and flow meter, within which the flow could be isolated when it was judged to contain fume. Similar to the Tedlar bag, an SPME fibre was then injected into the chamber and placed into an oven. This new system eradicated the presence of phenol and was used for the remaining fume analysis experiments. All the data in chapter 5 was inconclusive and none of the peaks observed on the chromatograms could be directly attributed to laser produced fume. It is important to note the dilution factor during laser irradiation, was that approximately 5000 chamber volumes passed through the sampling tube in the extraction flow. Also the sampling tube is a small proportion of the whole extraction flow, accounting for 1:69 of the total area. Therefore, for modest fume production, the sensitivity of the mass spectroscopy needs to be extremely high.

In order to increase the analyte concentration, a system that involved irradiation and accumulation of fume within a chamber before being drawn past an exposed SPME fibre was designed. This not only had the advantage of concentrating the fume before sampling, but also enabled irradiation under different atmospheres and pressures. However when irradiating with the IR laser, pressures could not exceed 0.33 bar above or below atmospheric pressure due to the salt windows used in the chamber. Particulates were collected and observed when the ITO thin

films were irradiated under a 130mJcm^{-2} XeCl laser regime. The particulates were captured on adhesive witness plates and observed to be 40nm ITO particle clusters via SEM and EDXA.

The ITO nanoparticles were found to be the most hazardous fume component in chapter 6. It was estimated that it would take approximately 30 minutes of irradiation to reach the TWA value in a 75m^3 room. In the same room it would take 1.6 hours of irradiation to reach the STEL value of ITO nanoparticles. A flow rate of at least $150\text{m}^3/\text{hr}$ is advised to avoid dangerous exposure to any chemicals. Exposure to nanoparticles should not occur however as the release of nanoparticles signifies damage to the conductive tracks of the irradiated material and therefore would reduce the conductivity. Consequently, the nanoparticle hazard primarily comes from ablative patterning and not laser sintering. Any organic material released as fume would be dealt with by the activated charcoal aspect of an LEV filter.

Originally, the SPME fibre and Tedlar bag system was chosen for sensitivity and due to preliminary studies. However, as the detection of phenol was attributed to contamination from the Tedlar bag, a glass and metal system was designed. This system proved successful in avoiding cross-contamination. Also if on-site fume analysis was required to detect any hazards in a manufacturing environment, a Tedlar bag may not be rugged enough to travel to the analysis facility. A system that is more rugged however and can collect a large mass range of analytes is thermal desorption tubes as mentioned in section 2.3. These would be stable and robust enough to be sent by post, and also enable easy comparison of fume data.

Future work will consider the application of this technique to the problems posed here.

The overall mitigation plan this research has lead to is a local exhaust ventilation system with a three stage filter including pre-filter, HEPA filter, and activated charcoal. The LEV should be capable of a flow rate of at least $150\text{m}^3/\text{hr}$ which is easily achieved with commercially available units containing these filters. Personal monitoring should also be worn to detect any nanoparticles.

The work in this thesis could be taken forward by developing a suitable process for on-site fume. Laboratory experiments should be undertaken by including the thermal desorption tubes within the secondary arm of the isokinetic sampling system in place of the glass chamber. The GC-MS chromatograms could then be compared for the SPME and thermal desorption tube data. Also analysis of the air from a Tedlar bag with the thermal desorption tubes should be undertaken to explore the contamination issue further.

References

- [1] AILU, “Laser-based Manufacturing Applications : UK Roadmap-2014 October 2014,” Tech. Rep. October, Engineering and Physical Sciences Research Council, 2014.
- [2] IOP, “The health of photonics,” Tech. Rep. May, Institute of Physics, 2018.
- [3] D. T. Reid, C. M. Heyl, R. R. Thomson, R. Trebino, G. Steinmeyer, H. H. Fielding, R. Holzwarth, Z. Zhang, P. Del’Haye, T. Südmeyer, G. Mourou, T. Tajima, D. Faccio, F. J. Harren, and G. Cerullo, “Roadmap on ultrafast optics,” *Journal of Optics (United Kingdom)*, 2016.
- [4] H. Mayer and B. Gleich, “Measuring Criticality of Raw Materials : An Empirical Approach Assessing the Supply Risk Dimension of Commodity Criticality,” *Natural Resources*, vol. 6, no. 1, pp. 56–78, 2015.
- [5] V. L. Frevel A. , Steffensen B., “Safe laser application requires more than laser safety,” *Optics and Laser Technology*, vol. 27, no. 1, pp. 1–4, 1995.
- [6] S. B. L. Vassie H. , Roach R. J. , Tyrer J. R., “Fumes generated during laser processing of polyvinyl chloride (PVC),” *Optics and Laser Technology*, vol. 27, no. 1, pp. 31–37, 1995.
- [7] J. P. Smith, C. E. Moss, C. J. Bryant, and A. K. Fleeger, “Evaluation of a smoke evacuator used for laser surgery,” *Lasers in Surgery and Medicine*, vol. 9, no. 3, pp. 276–281, 1989.

-
- [8] J. P. Smith, J. L. Topmiller, and S. Shulman, “Factors affecting emission collection by surgical smoke evacuators,” *Lasers in Surgery and Medicine*, vol. 10, no. 3, pp. 224–233, 1990.
- [9] L. Schultz, “An Analysis of Surgical Smoke Plume Components, Capture, and Evacuation,” *AORN Journal*, 2014.
- [10] R. J. Roach, E. A. Raymond, J. R. Tyrer, and B. L. Sharp, “The indexed assessment of fumes generated by high power laser material processing,” *Journal of Laser Applications*, vol. 10, no. 3, pp. 121–125, 2010.
- [11] R. Srinivasan, B. Braren, and R. W. Dreyfus, “Ultraviolet laser ablation of polyimide films,” *Journal of Applied Physics*, vol. 61, no. 1, pp. 372–376, 1987.
- [12] W. R. Creasy and J. T. Brenna, “Formation of high mass carbon cluster ions from laser ablation of polymers and thin carbon films,” *The Journal of Chemical Physics*, vol. 92, no. 4, pp. 2269–2279, 1990.
- [13] T. Götz and M. Stuke, “Short-pulse UV laser ablation of solid and liquid metals: Indium,” *Applied Physics A: Materials Science and Processing*, vol. 64, no. 6, pp. 539–543, 1997.
- [14] C. on Industrial Ventilation American, *Industrial Ventilation Manual*, vol. 552. American Conference of Governmental Industrial Hygienists, 1998.
- [15] J. Sims, P. A. Ellwood, and H. J. Taylor, “Pollutants from laser cutting and hot gas welding of polymer based materials,” *Annual Technical Conference - ANTEC, Conference Proceedings*, no. pt 1, pp. 1269–1273, 1994.

-
- [16] T. B. Reed and A. Das, "Handbook of biomass downdraft gasifier engine systems," techreport March, Solar Energy Research Institute, 1617 Cole Boulevard, Golden, Colorado 80401-3393, Mar. 1988.
- [17] Airflow Sciences Corp, "Isokinetic Particle Sampling," Mar. 2017. <http://www.airflowsciences.com/Services/FieldTesting/Isokinetic>.
- [18] M. B. Leach, *Radio frequency excited carbon dioxide laser processing of carbon fibre reinforced composites: experimental and theoretical analyses of the fume content and their expansion dynamics*. PhD thesis, University of Hull, July 2014.
- [19] B. Buszewski, T. Ligor, and J. Rudnicka, "SPME: Extraction of VOCs in human breath," techreport, Sigma Aldrich, July 2016. <http://www.sigmaaldrich.com/>.
- [20] Parker Balston, "Sample Analyzer Filters," techreport, Parker Balston, 4087 Walden Ave. Lancaster, NY 14086, July 2015.
- [21] J. H. Lee, S. M. Hwang, D. W. Lee, and G. S. Heo, "Determination of volatile organic compounds (VOCs) using tedlar bag/solid-phase microextraction/gas chromatography/mass spectrometry (SPME/GC/MS) in ambient and workplace air," *Bulletin of the Korean Chemical Society*, vol. 23, no. 3, pp. 488–496, 2002.
- [22] S. Aldrich, "Solid Phase Microextraction Fiber Assemblies Conditioning Instructions data sheet," techreport, Sigma Aldrich, 1999.

- [23] J. Caro and M. Gallego, “Environmental and biological monitoring of volatile organic compounds in the workplace,” *Chemosphere*, vol. 77, no. 3, pp. 426–433, 2009.
- [24] Eurofins, “Guide to Air Sampling,” techreport, Eurofins Air Toxics, Inc., Eurofins Air Toxics 180 Blue Ravine Road, Ste. B Folsom, CA 95630 USA, June 2014.
- [25] K. Kim and D. Kim, “A combination of Tedlar bag sampling and solid-phase microextraction for the analysis of trimethylamine in air: Relationship between concentration level and sample size,” *Microchemical Journal*, vol. 91, no. 1, pp. 16–20, 2009.
- [26] SKC, “Classic Tedlar Bags for VOCs,” 863 Valley View Road, Eighty Four PA 15330 USA, Apr. 2017. <https://www.skcinc.com/>.
- [27] C. A. Seneviratne, S. Ghorai, and K. K. Murray, “Laser desorption sample transfer for gas chromatography/mass spectrometry,” *Rapid Communications in Mass Spectrometry*, vol. 30, no. 1, pp. 89–94, 2015.
- [28] I. Mirzaee, M. Song, M. Charmchi, and H. Sun, “A microfluidics-based on-chip impinger for airborne particle collection,” *Lab on a Chip*, vol. 16, no. 12, pp. 2254–2264, 2016.
- [29] S. Palanco, S. Marino, M. Gabás, S. Bijani, L. Ayala, and J. R. Ramos-Barrado, “Micro- and nanoparticle generation during nanosecond laser ablation: correlation between mass and optical emissions,” *Optics Express*, vol. 22, no. 4, p. 3991, 2014.

- [30] M. S. Tillack, D. W. Blair, and S. S. Harilal, “The effect of ionization on cluster formation in laser ablation plumes,” *Nanotechnology*, vol. 15, no. 3, pp. 390–403, 2004.
- [31] N. Al-Dahoudi, H. Bisht, C. Göbbert, T. Krajewski, and M. A. Aegerter, “Transparent conducting, anti-static and anti-static-anti-glare coatings on plastic substrates,” in *Thin Solid Films*, 2001.
- [32] A. A. Serkov, H. V. Snelling, S. Heusing, and T. M. Amaral, “Laser sintering of gravure printed indium tin oxide films on polyethylene terephthalate for flexible electronics,” *Scientific Reports*, vol. 9, no. 1, p. 1773, 2019.
- [33] J. Puetz and M. A. Aegerter, “Direct gravure printing of indium tin oxide nanoparticle patterns on polymer foils,” *Thin Solid Films*, vol. 516, pp. 4495–4501, 2008.
- [34] Sigma-Aldrich, “Indium tin oxide MSDS,” techreport, Sigma Aldrich, 2019. <https://www.sigmaaldrich.com/safety-center.html>.
- [35] Sigma-Aldrich, “3-(trimethoxysilyl)propylmethacrylate (MPTS) MSDS,” techreport, Sigma Aldrich, Jan. 2018. <https://www.sigmaaldrich.com/safety-center.html>.
- [36] Sigma-Aldrich, “2-isopropoxyethanol MSDS,” techreport, Sigma Aldrich, 2019. <https://www.sigmaaldrich.com/safety-center.html>.
- [37] Lurederra, “Indium-free transparent conductive oxides for glass and plastic substrates,” techreport D2.4, Lurederra, Jan. 2017.

- [38] SCHOTT, “Schott Borofloat 33,” tech. rep., SCHOTT, Otto-Schott-Strasse 13 07745 Jena Germany, 2009. <http://psec.uchicago.edu/glass/borofloat33e.pdf>.
- [39] M. A. Aegerter, S. Heusing, M. de Haro Moro, C. M. Ahlstedt, and J. Puetz, “Gravure printing of transparent conducting ITO coatings for display applications,” *Advances in Optical Thin Films II*, vol. 5963, p. 59631E, 2005.
- [40] SCHOTT, “Borofloat 33 Thermal Properties,” techreport, SCHOTT, Otto-Schott-Strasse 13 07745 Jena Germany, 2019.
- [41] J. B. Pawliszyn, *Solid phase Microextraction: Theory and practice*. New York: John Wiley & Sons, 1997.
- [42] S. A. Wercinski, *Solid Phase Microextraction: A Practical Guide*. CRC Press, 1999.
- [43] Sigma-Aldrich, “Bulletin 928A: Solid Phase Microextraction Troubleshooting Guide,” techreport, Supelco, 2004.
- [44] Sigma-Aldrich, “Fibre Selection Guide,” *Sigma Aldrich*, 2019. <https://www.sigmaaldrich.com/technical-documents/articles/analytical/selecting-spme-fibers.html>.
- [45] D. A. Skoog, F. J. Holler, and S. R. Crouch, *Principles of Instrumental Analysis Sixth Edition*. 1998.
- [46] Restek, “GC Columns,” techreport, Restek, Ministry Wharf, Wycombe Rd, Saunderton, High Wycombe HP14 4HW, 2008.

- [47] Agilent Technologies, “Agilent 5975 inert GC / MS System Data Sheet,” tech. rep., Agilent, 2004.
- [48] Sigma-Aldrich, “Butyl methacrylate MSDS,” techreport, Sigma Aldrich, 2018. <https://www.sigmaaldrich.com/safety-center.html>.
- [49] Y. Luo, “Bond dissociation energies,” *CRC Handbook of Chemistry and Physics*, no. 89th ed., pp. 65–98, 2009.
- [50] Sigma-Aldrich, “Solid Phase Microextraction (SPME),” techreport, Supelco, 2017.
- [51] Purex, “Purex 400i product sheet,” techreport, Purex, 2018. <https://www.purex.co.uk/>.
- [52] J. Deng, Y. Yang, X. Wang, and T. Luan, “Strategies for coupling solid-phase microextraction with mass spectrometry,” *TrAC Trends in Analytical Chemistry*, vol. 55, pp. 55–67, 2014.
- [53] TWI, “Indium-Free Transparent Conductive Oxides for Glass and Plastic Substrates - Interim periodic report,” techreport, TWI, June 2018.
- [54] Engineering-360, “HEPA Filters and ULPA Filters Information,” techreport, IEEE GlobalSpec, 2019. <https://www.globalspec.com/>.
- [55] ILPI, “Glossary Table of Contents,” techreport, The MSDS Hyper Glossary, 2016. <http://www.ilpi.com/msds/ref/index.html>.
- [56] Wikipedia, “Measures of acute toxicity,” 2016. <https://en.wikipedia.org/wiki/>.

-
- [57] ESPI-Metals, “Indium tin oxide safety data sheet,” techreport, ESPI, 1050 Benson Way Ashland, Oregon 97520, July 2017. <https://www.espimetals.com/>.
- [58] ALFA, “3-Methacryloxypropyltrimethoxysilane Safety data sheet,” techreport, ThermoFischer Scientific, 2017.
- [59] JP DYECHEM, “Butyl methacrylate safety data sheet,” techreport, JP DYECHEM PVT LTD., 2001. <http://www.jpdyechem.com/>.
- [60] Sigma-Aldrich, “N,N-dimethylacetamide MSDS,” techreport, Sigma Aldrich, 2018. <https://www.sigmaaldrich.com/safety-center.html>.
- [61] Sigma-Aldrich, “Octamethylcyclotetrasiloxane safety data sheet,” techreport, Sigma Aldrich, 2019. <https://www.sigmaaldrich.com/safety-center.html>.
- [62] Sigma-Aldrich, “Phenol MSDS,” techreport, Sigma Aldrich, 2018. <https://www.sigmaaldrich.com/safety-center.html>.